ORIGINAL PAPER

Geochemistry of the Lower Cretaceous limestones in the Eastern Tethys Gyabula Formation (Himalaya, southern Tibet): implications for the depositional environment and tectonic setting

Qing Li[1,2,3] · Feng Ding[2,4] · Micha Ruhl[5] · Yongdong Wang[1] · Ying Li[2] · Lei Yang[2] · Kunzhi Xu[2] · Xiangang Xie[2,6]

Abstract

The Tibetan Himalaya region provides crucial sedimentary successions for studying the evolution of the eastern Tethyan depositional area. However, the palaeo-environmental conditions during the Early Cretaceous period in southern Tibet (Tethys Himalaya northern zone) are not well constrained. In this paper, we report on the major, trace, and rare earth elements, as well as the carbon and oxygen isotopic compositions of the limestone successions in the Lower Cretaceous Gyabula Formation of the Rongpo area. The obtained sedimentary rare earth element (REE) profiles suggest that the Rongpo area was situated on a passive continental margin during the Early Cretaceous. The integrated geochemical and sedimentological analyses and results suggest that the limestones were deposited in a non-open marine depositional environment, marked by anoxic conditions. The strong positive europium (Eu) anomalies (Eu/Eu* $= 1.77 \pm 0.07$), high SiO_2 contents (average $19.30 \pm 2.82\%$), and the negative $\delta^{13}C$ values and $\delta^{18}O$ values suggest that hydrothermal fluids may have impacted the Early Cretaceous Neo-Tethyan seawater geochemistry. The combined sedimentological and geochemical data provide new insights on the palaeo-environmental and tectonic setting of the Lower Cretaceous Neo-Tethyan successions of southern Tibet.

Keywords Southern Tibet · Early Cretaceous · Seawater geochemistry · Sedimentary/depositional environment · Tectonic setting

Introduction

The Cretaceous was a critical time period in the history of the Earth and was marked by significant climatic and environmental changes which were associated with the development of major greenhouse climate conditions (Bornemann et al. 2008; Wang 2013; Wang et al. 2014), global sea-level fluctuations (Haq et al. 1987; Haq 2014), continental and marine large igneous province (LIP) volcanism (Zhu et al. 2009), and the associated occurrence of widespread hydrothermal fluid activity (Kumar et al. 2017; Wang et al. 2017), oceanic anoxic events (Schlanger and Jenkyns 1976; Scholle and Arthur 1980; Jenkyns 1980, 2010; Li et al. 2016), oceanic red beds (Wagreich and Krenmayr 2005; Wang et al.

Responsible Editor: Attila Ciner

✉ Feng Ding
22847785@qq.com

✉ Yongdong Wang
ydwang@nigpas.ac.cn

[1] State Key Laboratory of Palaeobiology and Stratigraphy, and Center for Excellence in Life and Paleoenvironment, Nanjing Institute of Geology and Palaeontology, Chinese Academy of Sciences, Nanjing 210008, China

[2] College of Earth Sciences, Chengdu University of Technology, Chengdu 610059, China

[3] University of Chinese Academy of Sciences, Beijing 100049, China

[4] Key Laboratory of Tectonic Controls On Mineralization and Hydrocarbon Accumulation of Ministry of Natural Resources, Chengdu University of Technology, Chengdu 610059, China

[5] Department of Geology, Earth Surface Research Laboratory (ESRL), and Irish Centre for Research in Applied Geosciences (iCRAG), Trinity College Dublin, The University of Dublin, Dublin, Ireland

[6] School of Earth System Sciences, Tianjin University, Tianjin 300072, China

2005; Hu et al. 2006; Neuhuber et al. 2007; Li et al. 2011), and the last mass extinction event of the Phanerozoic (Russell 1982; Skelton et al. 2003). In China, marine sediments from the Cretaceous are well exposed on the southern Tibetan Plateau and are considered an ideal target for stratigraphical, palaeontological, palaeogeographical, and tectonic studies (Chen et al. 1993). Recently, detailed investigations on the Lower Cretaceous sedimentary archives of southern Tibet have focused on the local and regional bio- and lithostratigraphy, sea-level changes, and the palaeo-environmental, palaeobiological, and tectonic evolution of this area (Hu et al. 2008; Zhou et al. 1997; Liu and Li 2012; Yang et al. 2015; An et al. 2017; Huang et al. 2018). However, these studies have been centred on a geographically limited region in the Gyangzê, Kamba (Gamba), and Dingri (Tingri) areas (Fig. 1b) (Yu et al. 1983; Xu and Mao 1992; Yin and Wang 1998; Wang et al. 2000; Wang et al. 2005; Hu et al. 2006; Yue et al. 2003, 2006; Xia et al. 2008; Chen et al. 2008; Xiong et al. 2010; Gao et al. 2011; Li et al. 2016; Zhang et al. 2017; Hu et al. 2017). The few studies that have

been conducted considering the Rongpo area have provided stratigraphical and palaeogeographical constraints and an understanding of the fossil biota, sedimentary facies, and palaeobiogeography of this region (e.g. Wang 1984; Searle et al. 1987; Zhou et al. 2004; Xia et al. 2005, 2008; Cui et al. 2015). Moreover, it is controversial on the early Cretaceous palaeo-environmental conditions in southern Tibet. Previous study documents that it is an oxic marine environment (Xiong et al. 2010), while others suggest it is an anoxic condition (Yue et al. 2006) in southern Tibet. In addition, some thought that the carbonates of early Cretaceous in southern Tibet deposited on shelf or continental slope facies (Searle et al. 1987; Yue et al. 2003; Xia et al. 2008), while others considered they deposited on deep ocean (Yu et al. 1983; Li et al. 2016). Therefore, it's necessary to discuss the coeval palaeo-environmental conditions in the Rongpo area.

Here, we report comprehensive geochemical analyses (major and trace element concentrations and carbon and oxygen stable isotopes) of the Lower Cretaceous argillaceous limestones of the Gyabula Formation in the Rongpo region

Fig. 1 (Colour online) **a** Tectonic units of the Tibetan Plateau (simplified from Huang et al. 2019); **b** a sketch map of the Himalayan–Tibetan orogen, showing the location of the study area (modified after Hu et al. 2008; Lang et al. 2018)
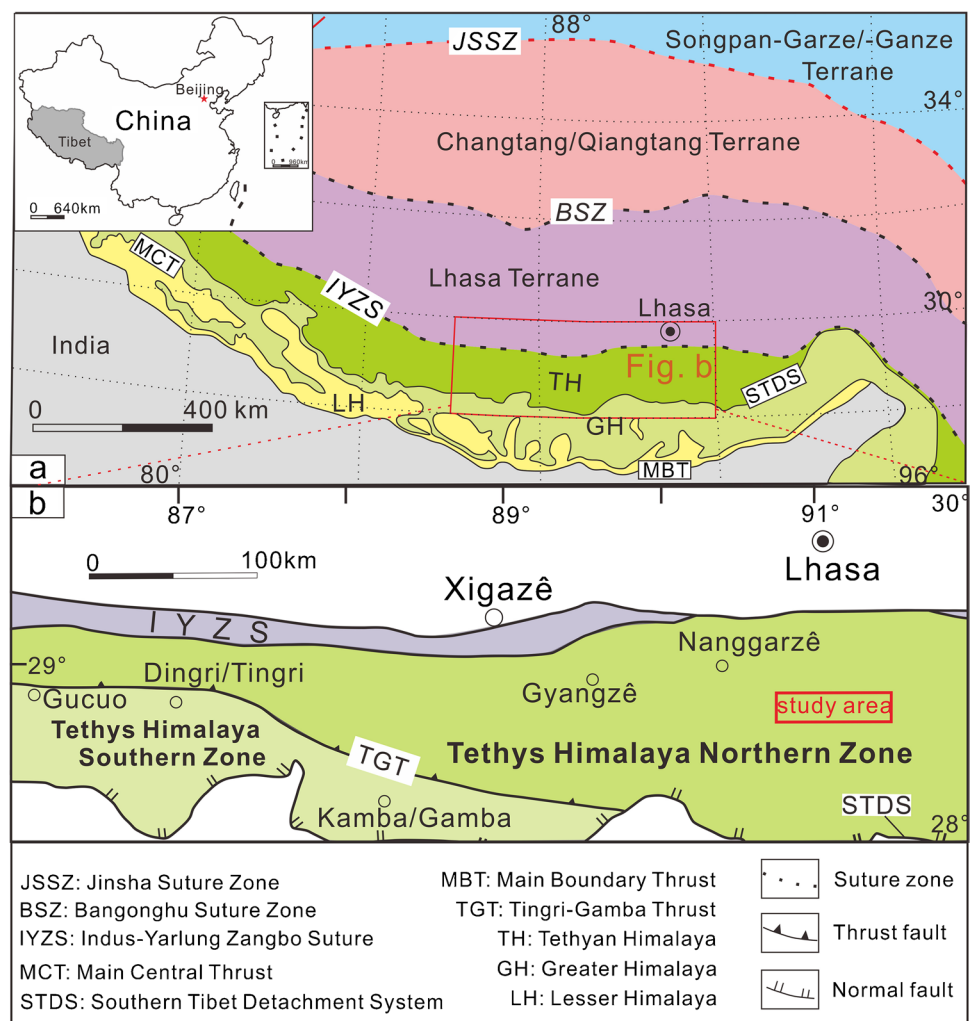
and provide constraints on the Rongpo depositional environment and tectonic evolution in Early Cretaceous, which is significant in shedding light on the palaeo-environmental and tectonic setting of the Lower Cretaceous successions of southern Tibet along the eastern Neo-Tethys.

Geologic setting and stratigraphy

The study area is located in the Tibet (southern Tibet) of southwest China (Fig. 1a). The Tibetan Plateau, which is located in the eastern part of the Tethys tectonic domain, is mainly composed of four continental terranes. From north to south, these are the Songpan-Garze (Songpan-Ganze), Changtang (Qiangtang), Lhasa, and Himalaya terranes, which are divided by the Jinsha suture zone (JSSZ), the Bangonghu suture zone (BSZ), and the Indus-Yarlung Zangbo suture (IYZS), respectively (Fig. 1a) (Yin and Harrison 2000; Huang et al. 2019). The Himalaya is located between the Main Boundary Thrust (MBT) to the south and the Indus-Yarlung Zangbo suture (IYZS) to the north. It consists of three tectonic entities from north to south, the Tethyan Himalaya (TH), the Greater Himalaya (GH), and the Lesser Himalaya (LH), which are separated by the Southern Tibet Detachment System (STDS) and the Main Central Thrust (MCT) (Fig. 1a) (Zhu et al. 2009; Li et al. 2016). The Tethyan Himalaya (Gansser 1964) is delimited between the Indus-Yarlung Zangbo suture (IYZS) and the Southern Tibet Detachment System (STDS) (Fig. 1a). Tectonically, the Tethyan Himalaya belongs to the Indian continental plate (northern Gondwanaland) and is subdivided into two zones by the Tingri-Gamba Thrust (TGT), i.e. the northern zone

and the southern zone (Fig. 1b) (Hu et al. 2008; Wang et al. 1996).

The study area is in the Rongpo region (N28°40′–28°50′, E90°45′–91°30′), which belongs to the Tethys Himalaya North Zone (Fig. 1b). It is located approximately 25 km southeast of Nanggarzê town, which lies within the Shannan Prefecture in the southern part of the Xizang Autonomous Region in southwest China. Mesozoic strata are widely developed and exposed in this region, including the Middle Jurassic Zhela Formation (J_2z), the Upper Jurassic Weimei Formation (J_3w), the Upper Jurassic–Lower Cretaceous Sangxiu Formation (J_3–K_1s), the Lower Cretaceous Gyabula Formation (K_1j), and the Upper Cretaceous Zongzhuo Formation (K_2z) (Fig. 2).

The Lower Cretaceous Gyabula Formation is the dominant succession in this region with extensive outcropping deposits (Fig. 2). Regional folds in this area suggest that the strata in the Gyabula Formation formed along a northwest–southeastern orientation. The Gyabula Formation conformably follows the underlying Upper Jurassic–Lower Cretaceous Sangxiu Formation (J_3–K_1s) and has an angular unconformity with the overlying Upper Cretaceous Zongzhuo Formation (K_2z), due to the local structures and movements that result from faulting (Fig. 2). The Sangxiu Formation is a rock association that is composed of basic–intermediate volcanic rocks, pyroclastic rocks, and argillaceous rocks.

The lithology of the Gyabula Formation is a complex association of primary dark grey shales and mudstones, secondary marlstone, limestone, and yellow greyish siltstone, as well as sandstone, which alternate with thin silty mudstones and muddy siltstones, as well as argillaceous and sandy lenses. The dark grey shales, which are interbedded with
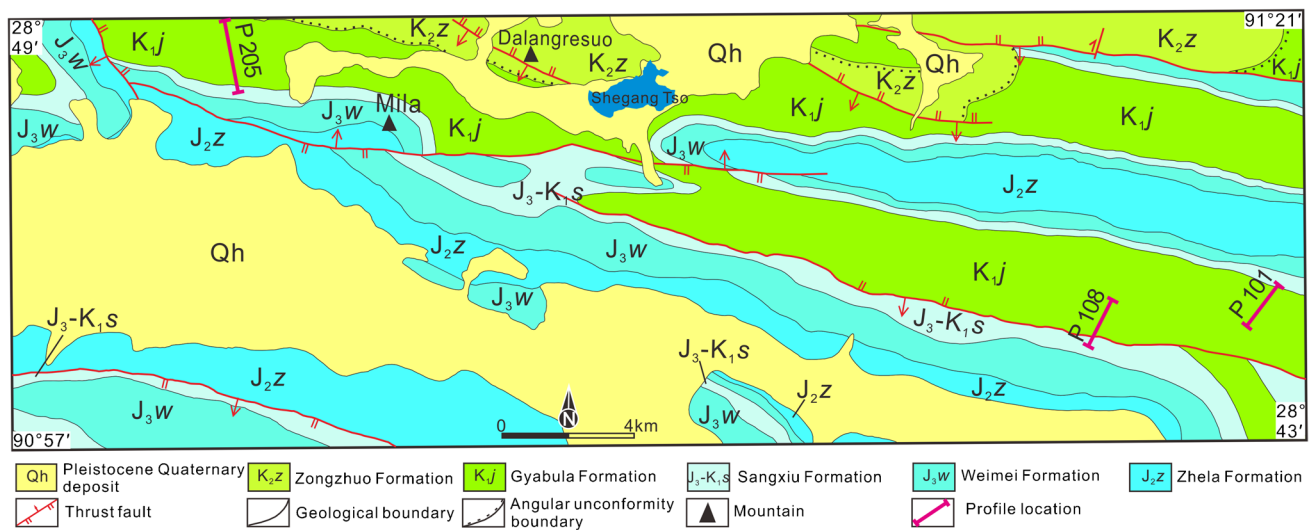

Fig. 2 (Colour online) Regional geological map of the study area, including the location of the sampled profile

mudstones and limestones, developed horizontal beddings (Fig. 3a–c), leading to lamellation and slight ferritization on the weathered surface of the shale. Belemnite fossils are predominant in the black-grey shales, and ammonite fossils also occur in some of the outcrops studied; however, the latter are poorly preserved.

Limestones are mainly found interbedded between mudrocks and shales, sometimes appearing as lenticles in the shale. The unweathered limestones (Fig. 3d–f) are marked by a microcrystalline texture under the microscope (Fig. 3g–h) and are grey to dark grey in colour, while the weathered surfaces of the limestones are marked by a grey brownish colour. The limestone mainly consists of microcrystaline calcite in the form of subhedral grains (approximately 0.03 mm in diameter), which account for approximately 80% of the matrix. The limestone facies

contain some bioclasts, as well as fossil algae and gastropods. The remaining 20% of the matrix is composed of irregular tiny micrite grains and minor argillaceous impurities (Fig. 3g–h).

The fossils that were reported in the Gyabula Formation include ammonites, such as *Thurmanniceras*, *Subthurmannia*, *Sarasinella*, *Calliptychoceras*, *Kilianella*, *Neocomites*, *Blanfordiceras*, *Spiticeras*, *Eulytoceras*, *Pseudohaploceras*, *Oxytropidoceras*, *Beudanticeras*, and *Douvilleiceras* cf. *mannilatum*; bivalves, such as *Inoceramus* (*Mytiloides*) *everesti*; and brachiopoda, such as *Peregrinella multicarinata*. These fossil biota are indicative of the Berriasian and Albian aspects of this formation. Therefore, the age of the Gyabula Formation is biostratigraphically limited to within the Early Cretaceous (Berriasian and Albian) (Xia and Liu 1997).

Fig. 3 (Colour online) Macro- and microphotographs of the Gyabula Formation: **a–f** outcrop photos of the Gyabula Formation; **g–h** plane and cross-polar images of the limestone microsections studied here
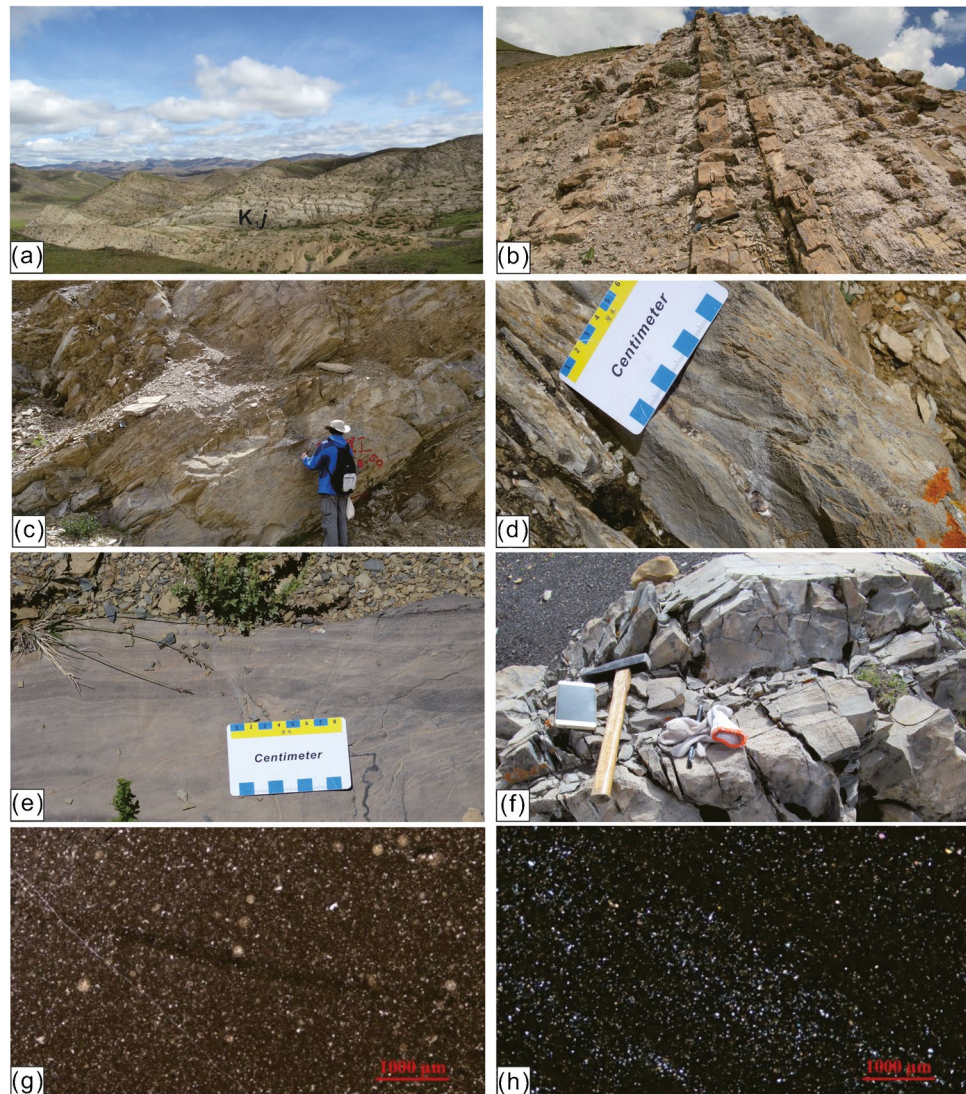
Sampling and analytical methods

The limestone samples were collected from three stratigraphic sections (profile 101, profile 108, and profile 205) which comprise the Lower Cretaceous Gyabula Formation in the Rongpo area (Fig. 4 and Table 1), based on the sampling strategies of fresh limestone outcrops. The collected,
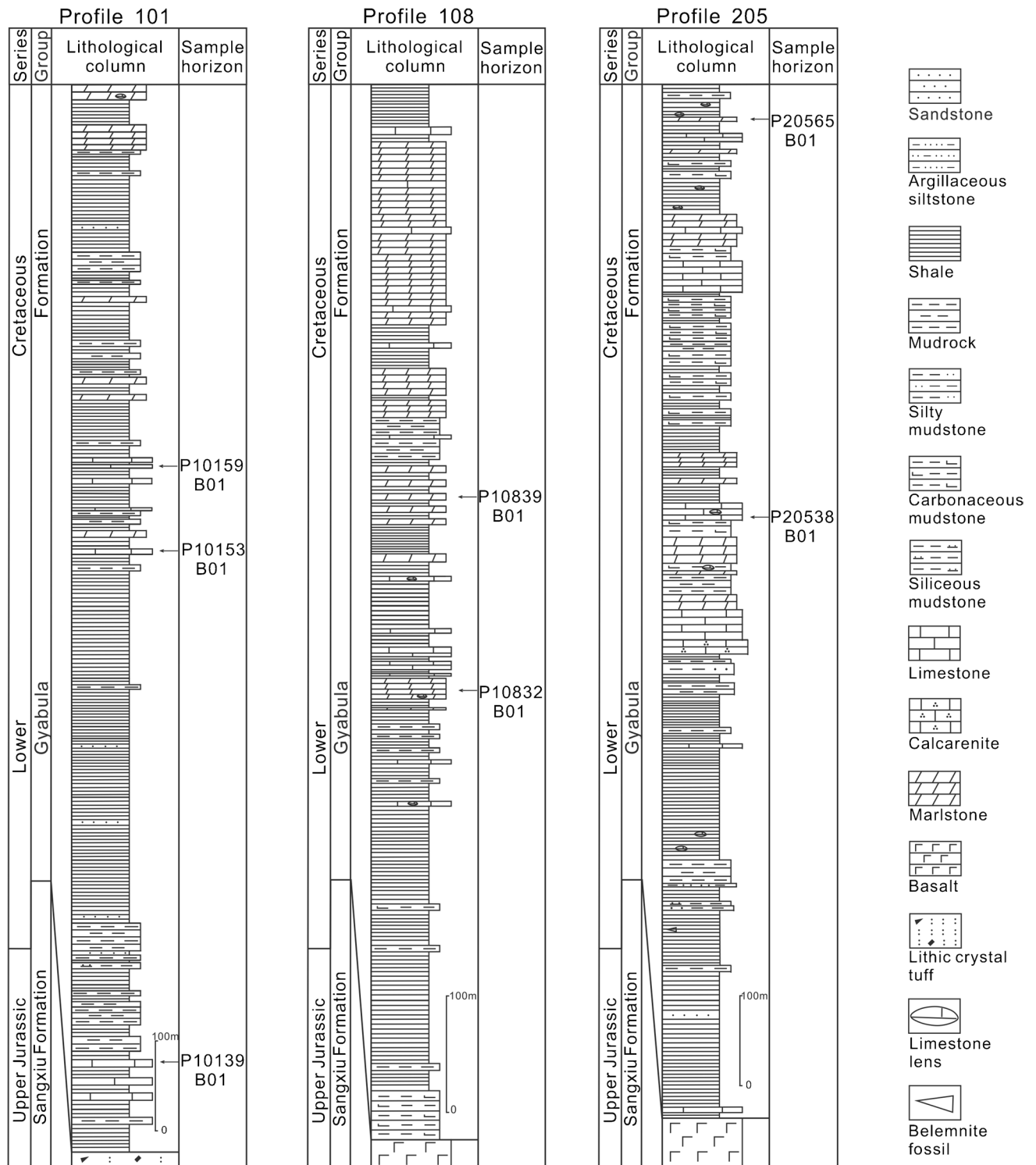

Fig. 4 Stratigraphic section and sample intervals in the Gyabula Formation of the Rongpo area

Table 1 Major element ($\times 10^{-2}$), trace element ($\times 10^{-6}$), and REE ($\times 10^{-6}$) data from the limestones in the Gyabula Formation

Samples (limestones)	P10139B03	P10153B01	P10159B01	P10832B01	P10839B01	P20538B01	P20565B01
Major elements ($\times 10^{-2}$)							
SiO_2	30.77	12.52	6.46	25.39	19.58	18.20	22.16
TiO_2	0.47	0.22	0.19	0.64	0.72	0.49	0.83
Al_2O_3	4.57	2.65	1.94	5.43	5.42	4.12	6.17
TFe_2O_3	5.68	1.51	0.89	3.48	2.94	2.75	3.72
MnO	0.35	0.08	0.11	0.44	0.74	0.64	0.94
MgO	1.27	1.33	0.98	0.82	0.83	0.62	0.73
CaO	29.82	43.45	48.79	33.37	36.52	37.36	33.28
Na_2O	0.38	0.95	0.86	1.26	2.15	1.03	1.72
K_2O	0.34	0.23	0.08	0.54	0.23	0.44	0.65
P_2O_5	0.22	0.28	0.15	0.10	0.12	0.13	0.16
LOI	25.95	36.28	39.34	28.36	30.54	33.56	29.13
Total	99.84	99.49	99.79	99.83	99.78	99.35	99.48
m	27.90	50.21	50.51	15.11	15.23	15.04	11.77
Trace elements ($\times 10^{-6}$)							
V	63.0	29.3	40.1	100	80.0	64.1	89.7
Cr	46.6	20.1	21.1	63.4	72.3	51.7	77.6
Co	11.1	4.87	8.94	10.1	10.2	9.83	11.4
Ni	41.2	10.8	6.93	22.2	14.1	16.4	21.3
Cu	29.0	7.42	7.75	15.8	11.2	15.6	12.9
Ga	5.93	3.90	1.45	8.01	5.83	6.28	9.46
Rb	14.7	9.05	3.50	19.4	8.38	21.1	27.2
Sr	393	427	584	1032	594	396	412
Y	18.0	6.47	9.51	14.9	14.0	14.9	15.7
Zr	77.0	90.0	38.3	98.7	68.6	85.5	122
Nb	12.0	6.77	3.65	9.92	6.10	10.2	13.5
Cd	0.05	0.03	0.03	0.03	0.05	0.03	0.05
Cs	0.72	0.54	0.23	0.98	0.38	1.06	1.14
Ba	297	69.3	49.0	110	103	126	111
Hf	2.53	2.79	1.19	1.82	1.80	2.81	3.59
Ta	0.69	0.39	0.20	0.57	0.37	0.47	0.69
Pb	5.77	4.32	2.79	5.83	3.90	7.10	8.74
Th	3.38	2.60	1.18	2.84	1.60	3.03	3.47
U	0.63	0.27	0.21	0.58	0.34	0.65	0.62
Mn	2742	606	824	3423	5735	4924	7260
Sr/Ba	1.32	6.16	11.92	9.38	5.75	3.15	3.71
Mn/Sr	6.98	1.42	1.41	3.32	9.66	12.43	17.63
Zr/Y	4.28	13.91	4.02	6.63	4.90	5.73	7.78
V/(V + Ni)	0.60	0.73	0.85	0.82	0.85	0.80	0.81
Rear earth elements ($\times 10^{-6}$)							
La	20.3	12.6	11.1	26.8	19.4	26.0	33.9
Ce	37.1	25.3	23.4	57.9	32.9	53.0	64.5
Pr	4.00	3.07	2.70	6.90	3.73	6.58	7.90
Nd	18.5	13.7	12.4	31.5	16.8	29.1	34.3
Sm	3.82	2.58	2.78	5.82	3.38	5.50	6.01
Eu	1.44	0.68	0.90	2.01	1.15	2.11	1.86
Gd	3.69	2.10	2.52	4.86	3.11	4.45	4.99
Tb	0.57	0.29	0.39	0.70	0.49	0.61	0.69
Dy	2.81	1.24	1.76	3.05	2.48	2.69	3.13
Ho	0.53	0.22	0.30	0.53	0.46	0.46	0.53

Table 1 (continued)

Samples (limestones)	P10139B03	P10153B01	P10159B01	P10832B01	P10839B01	P20538B01	P20565B01
Er	1.36	0.59	0.79	1.44	1.24	1.26	1.43
Tm	0.18	0.07	0.10	0.17	0.16	0.19	0.20
Yb	1.35	0.63	0.71	1.37	1.38	1.11	1.12
Lu	0.17	0.06	0.09	0.15	0.14	0.16	0.17
δEu	1.90	1.45	1.67	1.86	1.72	2.11	1.69
δCe	1.30	1.09	1.20	1.15	1.17	1.05	1.04
δLa	1.99	1.41	1.59	1.46	1.81	1.32	1.34
δGd	0.90	0.93	0.87	0.91	0.91	0.94	0.97
δPr	0.89	0.96	0.92	0.94	0.93	0.98	0.98
Y/Ho	34.12	29.48	31.77	28.02	30.59	32.34	29.28
(La/Yb)$_{PAAS}$	1.11	1.48	1.15	1.44	1.04	1.74	2.23
(La/Ce)$_{PAAS}$	1.14	1.04	0.99	0.97	1.23	1.02	1.09
(Pr/Yb)$_{PAAS}$	0.95	1.55	1.21	1.60	0.86	1.90	2.25
(Pr/Sm)$_{PAAS}$	0.66	0.75	0.61	0.74	0.69	0.75	0.83
(Sm/Yb)$_{PAAS}$	1.44	2.08	1.99	2.15	1.24	2.53	2.72
Ce$_{anom}$	− 0.06	− 0.05	− 0.03	− 0.03	− 0.09	− 0.05	− 0.06
∑REE	113.82	69.61	69.42	158.19	100.74	148.17	176.37
L/H	3.70	6.80	4.32	6.64	4.18	6.34	7.35

$TFe_2O_3 = Fe_2O_3 \, (wt\%) + 1.111 * FeO \, (wt\%)$

LOI = loss on ignition

$m = (100 \times MgO) / Al_2O_3$

$\delta Eu = [Eu/(0.67Sm + 0.33\,Tb)]_{PAAS}$

$\delta Ce = [Ce/(2Pr\text{-}Nd)]_{PAAS}$

$\delta La = [La/(3Pr\text{-}2Nd)]_{PAAS}$

$\delta Gd = [Gd/(2\,Tb\text{-}Dy)]_{PAAS}$

$\delta Pr = [2Pr/(Ce + Nd)]_{PAAS}$

$Ce_{anom} = log\,[3Ce_n/(2La_n + Nd_n)]$

LREEs including La, Ce, Pr, Nd; HREEs including Ho, Er, Tm, Yb, Lu, plus Y

L/H = LREEs/REEs

non-weathered limestone samples were cut in the lab in order to examine the microstructure.

The major and trace elements, as well as rare earth element (REE) concentrations, were analysed at the Test Center of the Southwest Metallurgical Geology Institute in Chengdu, China. The major element contents were tested using an AxiosX fluorimeter with the GB/T14506.28–2010 and DZG20-02 as reference standards (with an analytical precision of ± 1%). Trace elements were analysed using an iCAP6300 simultaneous spectrometer and the NexLON 300 × ICP-MS and AxiosX fluorimeter, with DZG20-02 and DZG20-06 as reference standards. The REEs were determined using a NexLON 300 × ICP-MS and are reported relative to the DZG20-06 standard. Based on the regular analyses of the reference standards, the analysis of the trace elements and REEs comprises an error < 2% error. All tests were conducted at laboratory conditions of 23 ℃ and 59% humidity.

The carbon ($\delta^{13}C_{Carb}$) and oxygen ($\delta^{18}O_{Carb}$) isotope values of the carbonate rock samples were analysed at the Geology Testing Center for Nuclear Industry in Beijing and the Experimental Technologies Center of Nanjing Institute of Geology and Palaeontology, Chinese Academy of Sciences, Nanjing, using a MAT-253 Gas Isotope Ratio Mass Spectrometer, using the phosphoric acid method (DZ/T 0184.17–1997), with an analytical precision of $\delta^{13}C_{V\text{-}PDB} \pm 0.1‰$ and $\delta^{18}O_{V\text{-}PDB} \pm 0.2‰$ in Beijing, and with standard errors less than 0.04‰ ($\delta^{13}C_{V\text{-}PDB}$) and 0.08‰ ($\delta^{18}O_{V\text{-}PDB}$) respectively.

Results

Major elements

The results of major, trace, and REE concentrations in the studied samples are summarized in Table 1. The

SiO_2 and CaO contents change greatly in the profiles that comprise the Gyabula Formation (profiles 101, 108, and 205) (Fig. 4), with 6.46–30.77% SiO_2 and 29.82–48.79% CaO. Smaller variations were observed in the Al_2O_3 and total Fe_2O_3 (TFe_2O_3) concentrations, at 1.94–6.17% and 0.89–5.68%, respectively. The concentrations of other oxides, such as MgO, K_2O, Na_2O, P_2O_5, TiO_2, and MnO, vary only slightly between samples.

Trace elements

The Sr/Ba ratio in the studied limestone samples varies in the range of 1.32–11.92 (Fig. 6b), with an average value of 5.91 ± 1.29. The Mn/Sr ratio varies in the range of

1.41–17.63 (Fig. 5a), with an average value of 7.55 ± 2.14. The Zr/Y ratio varies in the range of 4.02–13.91, with an average value of 6.75 ± 1.20. The V/(V + Ni) ratio varies in the range of 0.60–0.85 (Fig. 6c), with an average value of 0.78 ± 0.03 (Table 1).

Rare earth elements

The REE + Y concentrations of all the limestones presented in Table 1 are normalized to the Post-Archaean Australian Shale (PAAS) composite (McLennan 1989). The anomalies associated with the lanthanum (La), cerium (Ce), europium (Eu), and gadolinium (Gd) elements were calculated, respectively, using the equations:
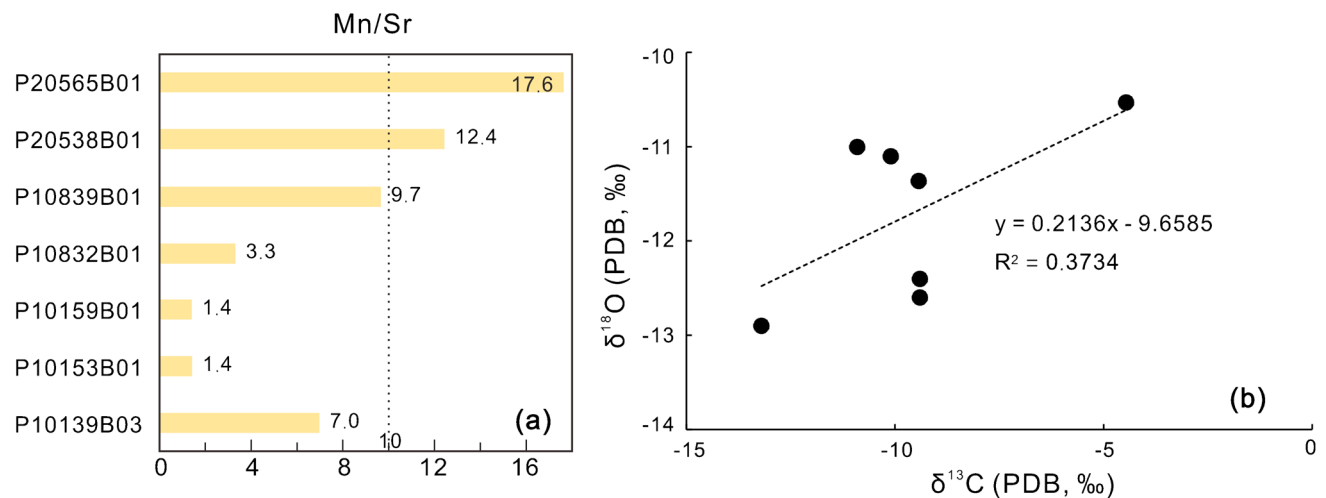

Fig. 5 (Colour online) **a** Ratios of Mn/Sr of the studied samples, evaluating the primary $\delta^{13}C$ abundances in the limestones of Rongpo area; **b** correlation of $\delta^{13}C_{PDB}$ and $\delta^{18}O_{PDB}$ values of samples from the studied profile, showing weak covariation

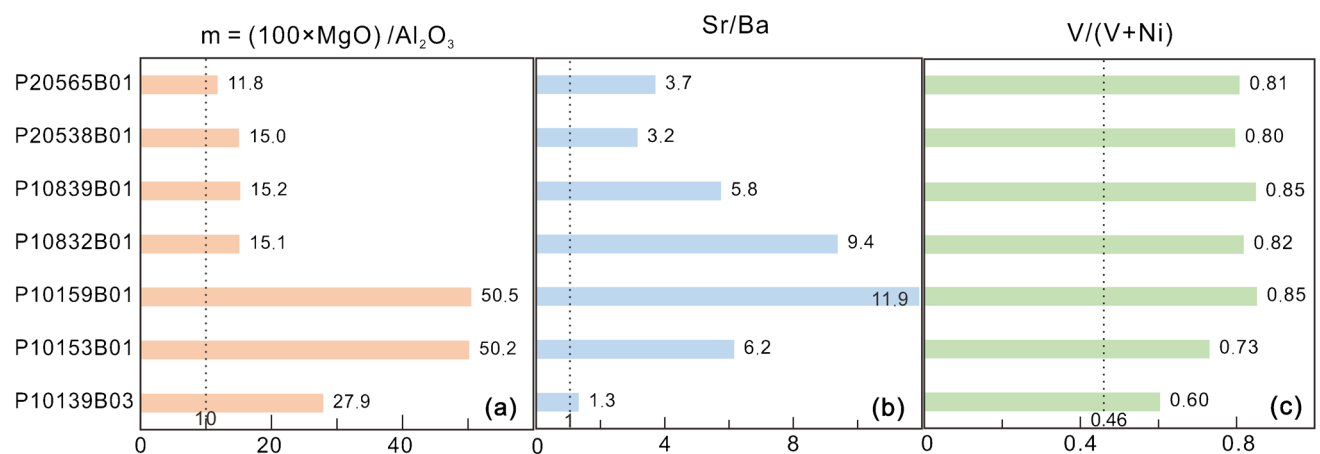**Fig. 6** (Colour online) **a** $m = (100 \times MgO)/Al_2O_3$ values from the limestone samples of the Rongpo area; **b** ratios of Sr/Ba of the Lower Cretaceous limestones that suggest a marine depositional environment for the Rongpo area; **c** ratios of V/(V + Ni) in the limestone samples studied, suggesting a relatively reduced marine depositional environment in the Rongpo area; the dashed line marks the indicator value mentioned in this paper

La/La* = [La/(3Pr-2Nd)]$_{PAAS}$; Ce/Ce* = [Ce/(2Pr-Nd)]$_{PAAS}$; Eu/Eu* = [Eu/(0.67Sm + 0.33 Tb)]$_{PAAS}$; and Gd/Gd* = [Gd/(2 Tb-Dy)]$_{PAAS}$ (Bolhar et al. 2004; Frimmel 2009).

The total REE contents in the limestone samples fall in the range 69.42×10^{-6} to 176.37×10^{-6}. The limestones of the Gyabula Formation are predominantly light REE (LREE)-enriched rather than middle REE (MREE) or heavy REE (HREE)-enriched ((Pr/Yb)$_{PAAS}$ = 1.48 ± 0.18; (Pr/Sm)$_{PAAS}$ = 0.72 ± 0.02; and (Sm/Yb)$_{PAAS}$ = 2.02 ± 0.19). Ce is showing moderately positive anomalies (Ce/Ce* = 1.15 ± 0.03); Eu shows strong positive anomalies (Eu/Eu* = 1.77 ± 0.07). La displays positive anomalies (La/La* = 1.56 ± 0.09), and Gd shows minor negative anomalies (Gd/Gd* = 0.92 ± 0.01).

Carbon and oxygen isotopes

The bulk rock carbon and oxygen isotope values of the studied limestone samples of the Gyabula Formation in the Rongpo area are all summarized in Table 2. The oxygen isotope PDB standard is also converted to the SMOW standard following the formula given by Coplen et al. (1983) ($\delta^{18}O_{PDB}$ (‰) = (0.97002 × $\delta^{18}O_{SMOW}$) − 29.98).

The $\delta^{13}C_{Carb}$ values of samples from profile 101 range from − 10.9 to − 9.4‰, while the samples in profile 205 (Table 2) present $\delta^{13}C_{Carb}$ values from − 13.2 to − 10.1‰. The $\delta^{18}O_{Carb}$ values vary from − 12.6 to − 11.0‰ in profile 101, while those in profile 205 vary from − 12.9 to − 11.1‰. The $\delta^{13}C_{Carb}$ and $\delta^{18}O_{Carb}$ values in profile 108 are − 4.5‰ and − 10.5‰ respectively. Relative to the nearby Gyangzê region (Hu, unpub. Ph.D. thesis, Chengdu University of

Technology, 2002), the samples studied here demonstrate more negative carbon and oxygen isotope values (Table 2).

Discussion

Evaluating the validity of geochemical data of samples

Before discussing the relationship between the geochemical data and environmental, as well as tectonic implications, it's necessary to evaluate the diagenetic effects on these data. Through microscopic observation on thin sections, we choose these samples without micro-cavities/cracks and dolosparite in the rocks (Fig. 3g–h), which indicate that they are not obviously affected by the post-depositional alteration of diagenesis. Mn/Sr ratios were sometimes used as an indicator of diagenetic alteration in carbonates (Brand and Veizer 1980; Derry et al. 1992, 1994). From the Gyabula Formation, the Mn/Sr ratios of samples (except two samples, P20538B01 and P20565B01) are less than 10 (Fig. 5a), which indicate that most of our samples retain primary $\delta^{13}C$ abundances. However, the Mn/Sr ratio is not always a good choice to trace the diagenetic alteration, for the samples even with higher Mn/Sr values (greater than 10) can still keep the relative abundances of $\delta^{13}C$ which reflect their related geochemical information (Li et al. 2009, 2013; Derry 2010). Hence, the covariation of the $\delta^{13}C$ and $\delta^{18}O$ values is used to evaluate the potential geochemical impact of diagenesis on bulk rock geochemistry (Veizer et al. 1999; Wynn and Read 2007). Usually, samples with $\delta^{18}O$ values below –10‰ were thought to be affected by diagenesis. All of the $\delta^{18}O$ values of the studied samples are less than –10‰. However, the C-O cross-plots of the studied samples from Rongpo show very weak covariation between $\delta^{13}C$ and $\delta^{18}O$ (Fig. 5b), which suggest that the carbon isotope composition of the studied samples has likely only been altered to minimal extent, if at all, likely representing the original isotopic information of seawater during deposition in Rongpo area of southern Tibet.

Lower Cretaceous sedimentary/depositional environments of the Eastern Tethys

Marine environment

The Early Cretaceous palaeo-environment in the Eastern Tethys, as recorded in the marine sedimentary successions of southern Tibet, is generally marked by oxygenated depositional conditions (e.g. Xiong et al. 2010) but also shows the occasional development of anoxic conditions (e.g. Yue et al. 2006). The geochemical analyses of the limestones of the Gyabula Formation in the Rongpo area presented in this study (Table 1) provide insight into local palaeo-environmental conditions during the Early Cretaceous.

Table 2 $\delta^{18}O$ and $\delta^{13}C$ data from the limestones of the Gyabula Formation in the Rongpo area

Area	Sample	Lithology	$\delta^{13}C$ (PDB, ‰)	$\delta^{18}O$ (PDB, ‰)	$\delta^{18}O$ (SMOW, ‰)
Rongpo	P10139B03	Limestone	− 9.4	− 11.4	19.2
	P10139-N01	Limestone	− 9.4	− 12.6	17.9
	P10139-N02	Limestone	− 10.9	− 11.0	19.6
	P10139-N03	Limestone	− 9.4	− 12.4	18.1
	P10839B01	Limestone	− 4.5	− 10.5	20.0
	P20538B01	Limestone	− 13.2	− 12.9	17.6
	P20565B01	Limestone	− 10.1	− 11.1	19.5

In modern sediments, m values (where the m value is defined as $m = (100 \times MgO)/Al_2O_3$) have an exponential relationship to the average (bottom) seawater salinity in a depositional environment, which increases alongside the water salinity (Zhang 1988; Zhang and Chen 1991; Jing et al. 2005). The m value of the limestone samples from the Gyabula Formation ranges from 11.77 to 50.51 (Table 1, Fig. 6a). m values that lie within the range of 10 (dashed line in Fig. 6a) to 500 may indicate a marine depositional environment (Zhang 1988; Jing et al. 2005), thus implying that these limestones likely formed under marine depositional conditions.

The concentration of trace elements and their relative abundance (or ratios) can also be suggestive of conditions in the depositional environment, changes in the relative sea level, and sedimentary provenance (Zhao 1989; Deng and Qian 1993; Yang et al. 2009). The ratio between the sedimentary concentrations of strontium (Sr) and barium (Ba), given as the Sr/Ba ratio, may be indicative of the depth of the water column, salinity, and/or the proximal vs distal nature of the depositional area, with Sr/Ba > 1 reflecting a marine environment, and Sr/Ba < 1, reflecting a terrestrial environment (assuming no diagenetic processes impacting on the original elemental composition of the host rock) (Jing et al. 2005; Yang et al. 2009). The average Sr/Ba values of the limestones in the Gyabula Formation are approximately 5.91 ± 1.29, which is indicative of a marine environment (Table 1; Fig. 6b). Furthermore, the depositional environment of the Gyabula Formation is marine, which is also testified by fossils, such as ammonites, bivalves, brachiopodas, and calcareous nannofossils (Wang et al. 2000; Zhou et al. 2004; Xia et al. 2008; Gao et al. 2011) and sequence stratigraphy (Chen et al., 1993; Cui et al. 2015).

Redox state of the depositional environment

The abundance of vanadium (V) relative to nickel (Ni), defined as the V/(V + Ni) ratio, can be indicative of the prevailing redox conditions in the depositional environment (Hatch and Leventhal 1992; Jones and Manning 1994). A sedimentary V/(V + Ni) ratio that is equal to or greater than 0.46 may suggest a reduced depositional environment, while a ratio lower than 0.46 may suggest an oxidized depositional environment. The V/(V + Ni) ratios of the studied Lower Cretaceous limestones in the Rongpo area are all above 0.46, suggesting a relatively reducing depositional environment (Fig. 6c). Organic-rich black shales are often deposited in a reducing depositional environment. The abundant coeval black or grey-black shales interbedded with the limestones of the Gyabula Formation in the Rongpo region provide further lithological evidence for predominantly reducing depositional conditions.

Limestones record the REE signatures of seawater in which they were precipitated (Nothdurft et al. 2004). The concentration of REEs in seawater is controlled by different input sources (such as terrestrial input from continental weathering and hydrothermal input) and scavenging processes that are related to depth, salinity, and oxygen levels (Elderfield 1988; Piepgras and Jacobsen 1992; Bertram and Elderfield 1993; Greaves et al. 1999). The distinctive character of the seawater REE pattern reflects the largely uniform trivalent behaviour of the elements (except Ce and Eu, which vary with oxygen levels) and the estuarine and oceanic scavenging processes (Nothdurft et al. 2004; Bolhar and Van Kranendonk 2007). However, the valence state of Eu and Ce can easily be affected by changes in the redox state of the depositional environment or the sedimentary pore space. Therefore, the sedimentary concentration of Eu and Ce is often fractionated from the other REEs (Nothdurft et al. 2004; Bolhar and Van Kranendonk 2007; Zhai et al. 2015).

The Ce anomaly has been used as an indicator of the redox state of the water column (e.g. de Baar 1983). Fractionated by the co-precipitation of metallic oxides under oxidizing conditions, Ce presents a negative anomaly in seawater (Wright et al. 1987). Conversely, under reducing conditions, Ce shows a positive anomaly in the REEs patterns of seawater. Therefore, variations in the sedimentary Ce concentrations can be used to estimate the redox state of the water column overlying the depositional environment. In this study, PAAS-normalized Ce displays moderate positive anomalies (with average values of 1.15 ± 0.03) (Table 1). Meanwhile, Wright et al. (1987) used a mathematical formula to constrain the enrichment or depletion factor of Ce as relative to La and Neodymium (Nd), defined by $Ce_{anom} = \log [3Ce_n/(2La_n + Nd_n)]$. In the formula, Ce_n, La_n, and Nd_n are normalized to chondritic values or to the North American Shale Composite Standard (Gromet et al. 1984). Sediments with $Ce_{anom} < -0.1$ are thought to represent formation in an oxidizing depositional environment, while sediments with $Ce_{anom} > -0.1$ are indicative of reducing depositional conditions (Wright et al. 1987; Nan et al. 1998). The Ce_{anom} values of the samples from the Lower Cretaceous Gyabula Formation in southern Tibet are all above -0.1 (-0.09 to -0.03, normalized to North American shale), further suggesting a reduced sedimentary/depositional environment, which is in agreement with the V/(V + Ni) values observed in the same samples.

Additionally, the distinctly positive Eu anomaly (Eu/Eu* = 1.77 ± 0.07) also indicates an anoxic depositional environment as it is caused by the reaction in which Eu^{3+} is reduced to Eu^{2+}, replacing the Ca^{2+} ions in the limestone.

Tectonic setting

Non-open ocean environment

Limestone geochemical studies were used to discriminate the tectonic setting of the basin in which the studied limestones are formed. The ratios of La/Ce, Ce/Ce*, Zr/Ti, and La/Sc in the limestones can be used as proxies to distinguish between the major tectonic and depositional environmental settings, such as oceanic plateaus, active or passive continental margins, and continental interior freshwater basins (Zhang et al. 2017). The REE and trace element geochemistry of the studied limestones were used to identify the tectonic setting of the Rongpo region, as compared to adjacent regions, such as Xigazê (Xigaze) (QB), Dingri (Tingri) (GB), Gêrzê (GZ), Coqên (WGZ), and Baishi (D1030).

The elements yttrium (Y) and holmium (Ho) have similar ionic radii and oceanic distributions. Owing to the differences in the complexation behaviour of these elements in seawater-derived inorganic ligands (mainly carbonate ions) on the surface of particulate matter, the present-day oceanic residence-time of Y in the global ocean is nearly twice as long as Ho (Nozaki et al. 1997). The fractionation of Y and Ho during weathering and the fluvial transport flux to the global ocean appears to be of minor influence on the relative abundance of Y and Ho in global seawater (Nozaki et al. 1997). However, Y is less effectively scavenged from seawater than any of the trivalent REEs. Therefore, the Y/Ho ratio in seawater is higher compared to freshwater environments (Nozaki et al. 1997). The limestones of the Rongpo area that are investigated in this study exhibit Y/Ho values of 30.80 ± 0.73, which are slightly higher than the value of PAAS (with Y/Ho values of 27.25) but much lower compared to the Y/Ho ratio of 60–90 in present-day global seawater (Frimmel 2009; Lawrence et al. 2006). Continental and marginal marine limestones also have different Ce/Ce*, $(La/Yb)_{PAAS}$, and $(La/Ce)_{PAAS}$ values compared to limestones that have formed in open marine environments (Fig. 7) (Zhang et al. 2017). The geochemical characteristics of the studied Lower Cretaceous limestones of the Rongpo area suggest that they formed in a non-open marine environment.

La, Ce, and praseodymium (Pr) anomalies, which are typically calculated as $Ce/Ce^* = [Ce/(0.5La + 0.5Pr)]_{PAAS}$ and $Pr/Pr^* = [2Pr/(Ce + Nd)]_{PAAS}$ (Van Kranendonk et al. 2003), can also be indicative of the conditions in the depositional environment. In our samples, both La and Ce show positive anomalies, which is in contrast with the typical REE signatures observed in open marine and non-marine (lagoonal) limestones (Fig. 8). Marine chemical sediments mainly show seawater-like REE + Y patterns (Nothdurft et al. 2004; Bolhar and Van Kranendonk 2007), which are characterized by light REE (LREE) depletion relative to heavy REEs (HREEs), a positive La anomaly, a negative Ce anomaly (de Baar 1991; Bau and Dulski 1996), and slight enrichments of Gd and Y in shale normalized diagrams (Zhang and Nozaki 1996; Bau 1996; Bau and Dulski 1996; Bolhar et al. 2004; Frimmel 2009). Additionally, observed seawater Y/Ho ratios are distinctively high (e.g. Bau 1996). In contrast, the samples from the Rongpo area are relatively rich in light REEs and have a slightly positive Ce and weakly negative Gd anomalies. Combined, this suggests that the samples in this study formed in a non-open marine sedimentary or depositional environment.

Passive margin

Limestones that formed in different tectonic and/or depositional settings can have different REE concentrations and signatures (Fig. 9), even the limestones from the same plate tectonic setting also have obvious undulation of REE concentrations but exhibit generally similar REE patterns (Zhang et al. 2017). Combined (Figs. 7 and 9b), we know that all our samples fall into the "Inland + Margin" area. In Fig. 9a–f, among the normalized REE + Y patterns passive margin (Fig. 9d) and Inland (Fig. 9e), it's easy to find that the patterns of the study samples (Fig. 9f) are similar to the main trend of passive margin(Fig. 9d), with obviously positive Eu anomaly and LREE enrichment. Therefore, based on our results, and in comparison to the REE signatures of adjacent regions, the Lower Cretaceous limestones of the Gyabula Formation in the Rongpo area likely formed in a similar setting as those in the Dingri (Tingri) region, which is located on a passive margin (Fig. 9a–f). Although the Xigazê (Xigaze) region is geographically closer to the present study area than Dingri (Tingri) (Fig. 1), the REE + Y patterns of limestone samples from Xigazê (Xigaze) are quite different from that of Rongpo, especially the relative concentrations of Eu and Y (Fig. 9a and f).

The Dingri (Tingri) region belongs tectonically to the southern zone of the Tethyan Himalaya, while the Rongpo region tectonically belongs to the northern zone. As they demonstrate similar REE + Y patterns (Fig. 9d and f), their depositional environments may have experienced similar tectonic and/or depositional settings on the Early Cretaceous passive margin. In the Early Cretaceous, a relatively stable environment may have developed along this passive margin in the Rongpo area, which may have enabled the formation of extensive marine grey-black shales and mudrocks, alternating with limestones, at the time.

Fig. 7 (Colour online) Ce/Ce*
vs (La/Yb)$_{PAAS}$ (**a**) and (La/
Ce)$_{PAAS}$ (**b**) in the Lower Cre-
taceous limestones deposited in
the Rongpo area
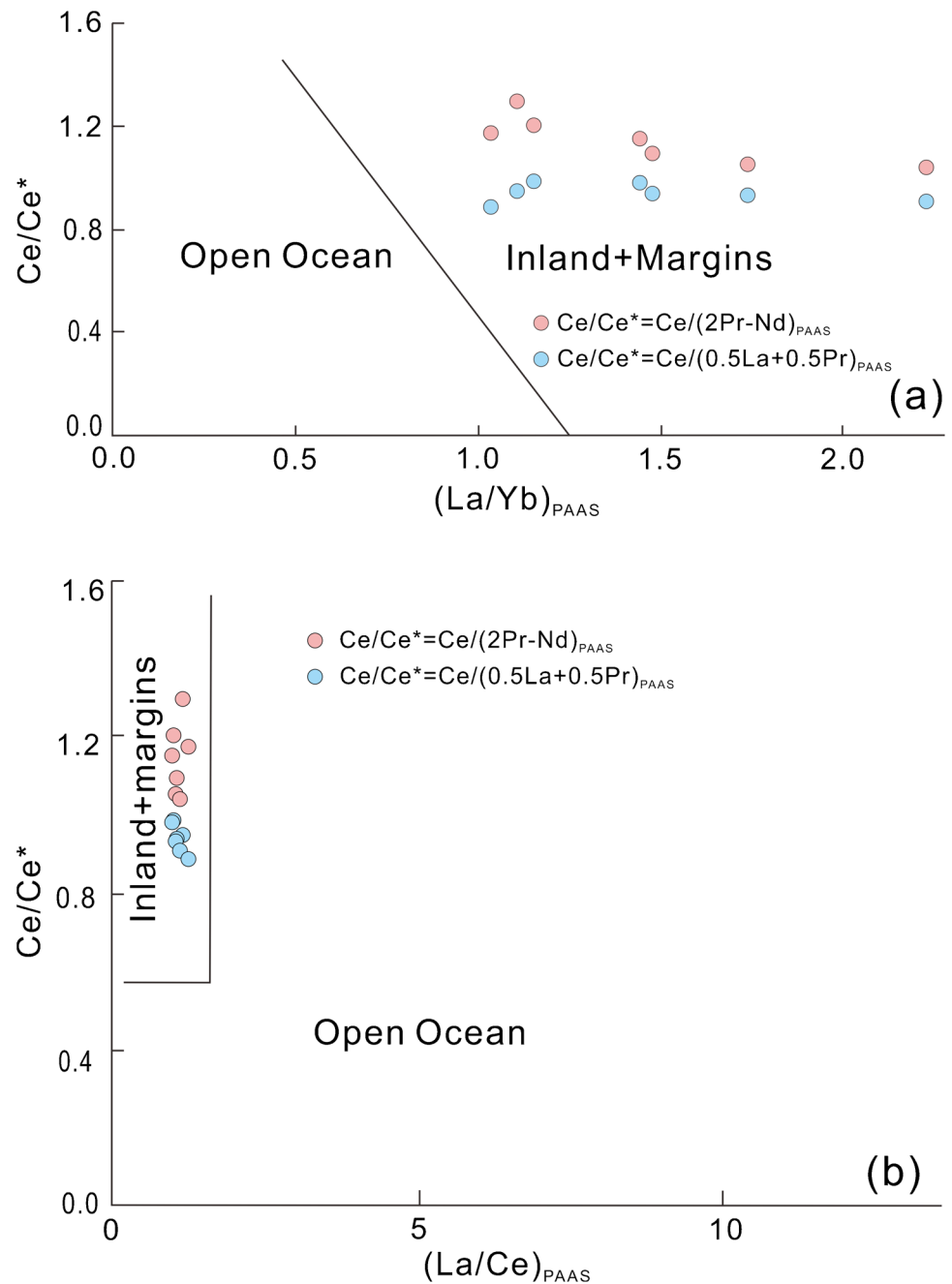
Influence of hydrothermal fluids

Eu anomalies

Eu generally shows a strong positive anomaly (Eu/Eu*
$_{PAAS}$ = 1.77 ± 0.07) in limestone sediments, because the
reduction of Eu^{3+} to Eu^{2+} allows Eu^{2+} to be replaced with
Ca^{2+} (Zhai et al. 2015). Several causes have been identified
to explain the Eu anomalies that are found in sedimentary

rocks, including the mixing of hydrothermal fluids (Bau
and Dulski 1999; Danielson et al. 1992; Derry and Jacob-
sen 1990; Michard et al. 1983), the mixing of Eu-rich water
that is leached from weathered rocks near the sedimentary
source, or the formation of Eu and Fe hydroxide complexes
(Van Kranendonk et al. 2003). However, no obvious correla-
tion is observed between the positive Eu anomalies and the
Fe hydroxides in the limestone samples (Table 1). Based on
the data collected in this study (six sandstone samples from
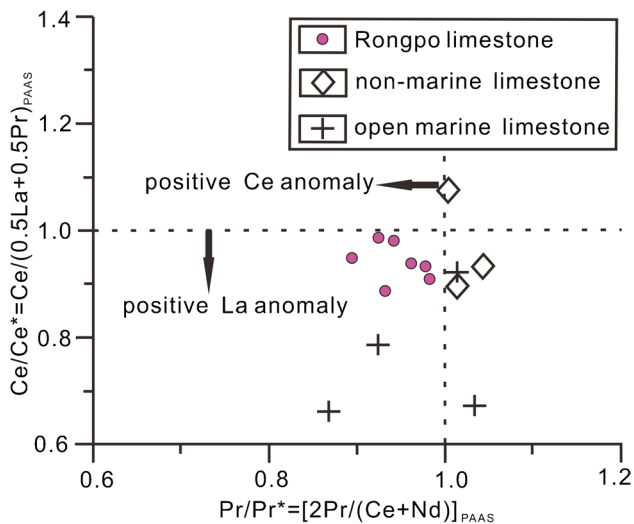
Fig. 8 (Colour online) Plot of $[Ce/Ce^*]_{PAAS}$ versus $[Pr/Pr^*]_{PAAS}$, showing La and Ce anomalies in the studied samples (non-marine data from Bolhar et al. 2007; open marine carbonate rocks data from Van Kranendonk et al. 2003)

the Gyabula Formation with Eu average 0.82 ± 0.09 are normalized by chondrite (Boynton 1984; Ding et al. unpub.), no positive Eu anomaly is apparent in the clastic rocks of the studied formation, which indicates that the clastic rocks were not contaminated with water containing large amounts of Eu that was sourced from continental weathering, affecting the sedimentary process. Therefore, we infer that the positive Eu anomaly in the limestones was not caused by the mixing of basin waters with Eu-enriched waters from leached Eu-enriched lithologies in the sedimentary source area. This leaves the possibility that the observed Eu anomalies reflect a supply of hydrothermal fluids. Probably, the hydrothermal fluids could provide the reduced gas, e.g. H_2S and CH_4, except for carbon source, which make Eu^{3+} reduced to Eu^{2+} and replace the Ca^{2+} ions in the limestone.

Rocks affected by hydrothermal fluid migration typically show similar REE signatures (Michard 1989), with positive Eu anomaly, enrichment of LREEs relative to the HREEs, and positive Y anomaly (Klinkhammer et al. 1994; Douville et al. 1999; Wheat et al. 2002). Interestingly, the REE + Y distribution pattern of the limestones in the Rongpo area (Fig. 10a) shows similar patterns to those of hydrothermal fluids (Fig. 10b), including a strongly positive Eu anomaly and positive Y anomaly. Because of this, the positive Eu anomaly observed in the limestone samples investigated in this study may have resulted from mixing with hydrothermal fluids.

The occurrence of Lower Cretaceous volcaniclastic sandstones (unweathered volcaniclastic grains in the sandstones) in the Gucuo region (Fig. 1b) (to the west of the Rongpo

area) (Powell et al. 1988; Patzelt et al. 1996; Chen et al. 2007; Hu et al. 2008) and mafic magma from the Early Cretaceous, such as the Comai (Comei) LIP (Zhu et al. 2009; Huang et al. 2018, 2019), is extensive within the Tethyan Himalayan belt. This suggests that magma activity or hotspots occurred during the Early Cretaceous, likely accompanied by extensive hydrothermal fluid systems. The hotspots have been indeed found in the eastern margin of Indian Plate in Cretaceous (Li and Jiang 2013). The Comai (Comei) LIP (N28° − 29°, E90°30′ − 92°), including the study area (N28°40′–28°50′, E90°45′–91°30′), is an evidence for hydrothermal fluid in Early Cretaceous (Zhu et al. 2009).

Carbon and oxygen isotopes

Previous studies have indicated that the carbon isotope values in the bulk rock carbonates that form in different sedimentary environments can vary distinctly (Rollinson 1993). Therefore, the carbon and oxygen isotopes can be applied to understand the limestone lithification (Hudson 1977). The values of $\delta^{18}O_{PDB}$ (and $\delta^{18}O_{SMOW}$) and $\delta^{13}C_{PDB}$ of the samples investigated in this study are plotted in Fig. 11. The red points represent the $\delta^{18}O$ value of the sample using SMOW as the standard, while the blue points represent the $\delta^{18}O$ value of the sample using PDB as the standard. It shows that most of our samples fall within the M-V (Mississippi Valley-type deposit) range, representing a range of values that are typically associated with low-temperature hydrothermal fluids. The Cretaceous hotspot that existed near the Comai (Comei) LIP (Li and Jiang 2013) does suggest that associated hydrothermal fluids may have impacted the geochemical signatures preserved in the studied samples. The Comai (Comei) LIP that was identified in the study area and active ~ 132–134 Ma and 136.9–143.5 Ma (Zhu et al. 2009; Huang et al. 2019) was likely linked to the Kerguelen mantle plume. Thermogenic methane, typically marked by very negative $\delta^{13}C$ values of ~ − 30‰, and likely associated with the mantle plume and LIP emplacement, may have impacted the carbon isotopic composition of the depositional environment and sedimentary pore space in which the carbonates formed. This likely caused the carbon isotopes in the carbonates to be very low, reaching as low as − 27.7‰ (Tong and Chen 2012).

Combined with the REE geochemistry of the studied samples, these results suggest that the composition of limestones of the Rongpo area was impacted or affected by hydrothermal fluids during its formation.

Furthermore, the negative $\delta^{18}O$ values may also be partly due to the elevated seawater temperature caused by the high temperature at the surface of the sea (Littler et al., 2011) or the warmer bottom waters (Wynn and Read 2007) that result from the presence of hydrothermal fluid.
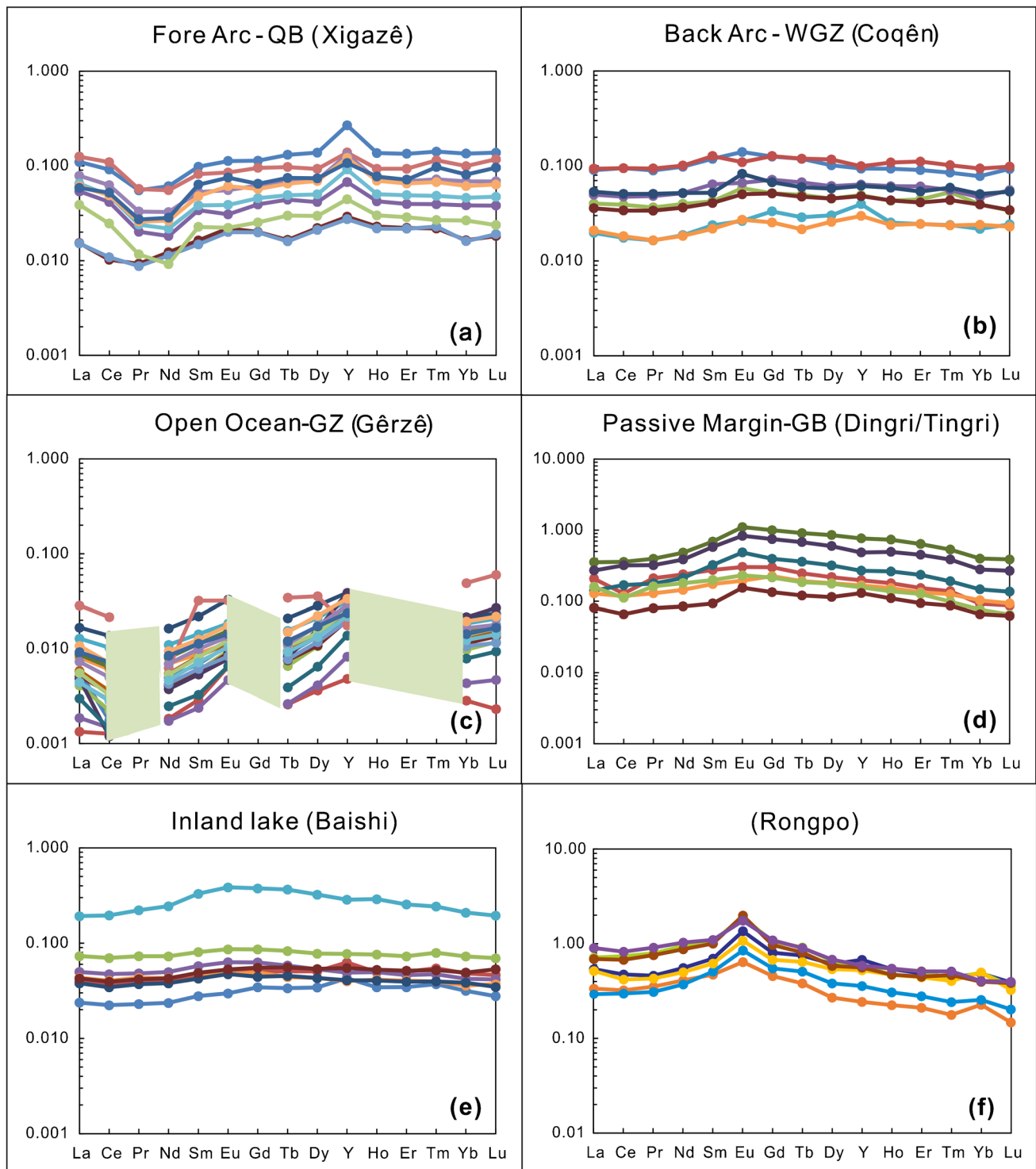
Fig. 9 (Colour online) PAAS-normalized (McLennan 1989) REE + Y concentrations of limestones that were deposited at various plate tectonic settings in Tibet, western China. Data in **a–e** is from Zhang et al. (2017); data in **f** is from this study

Evolution of the Upper Jurassic to the Lower Cretaceous Himalaya Neo-Tethys (Rongpo)

In the geological history of the Himalayas, the evolution of the Neo-Tethys played a critical role in controlling stratigraphic deposition (Guo et al., 2013; Liu and Einsele 1994). The Neo-Tethys formed between the Lhasa block and the Indian Plate, beginning with a rift stage during the Triassic (Liu and Einsele 1994). Based on the geochemical analyses of the Lower Cretaceous limestones from the Gyabula
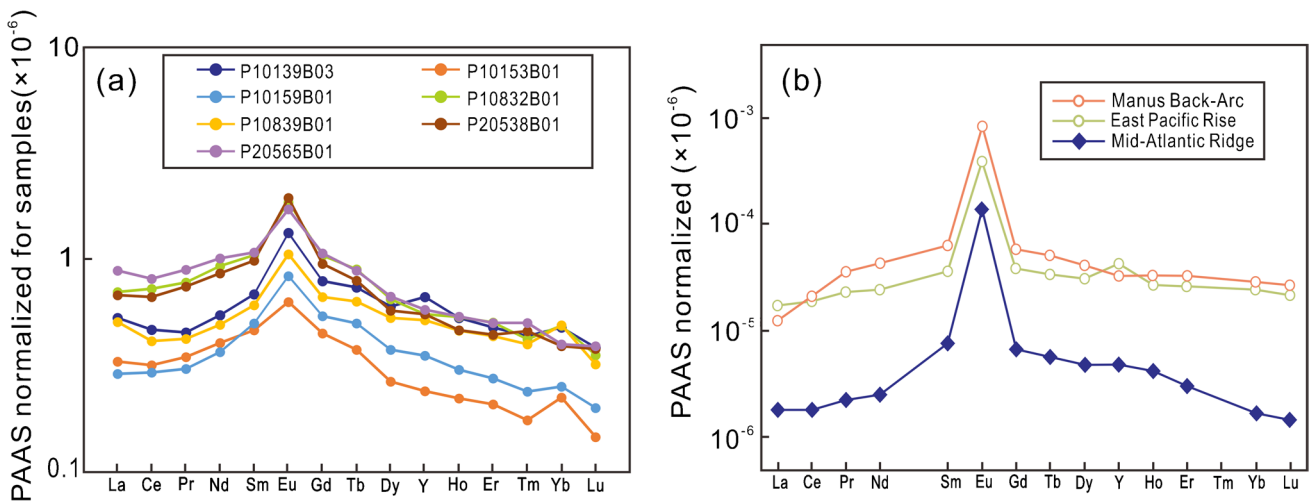
Fig. 10 a PAAS-normalized REE+Y patterns for samples from the Gyabula Formation; **b** modern hydrothermal fluid PAAS-normalized REE+Y patterns (cited from Van Kranendonk et al. 2003; Douville et al. 1999)

Fig. 11 (Colour online) δ^{18}O (SMOW and PDB scales) vs δ^{13}C plot showing the composition of carbonates from a variety of environments (Rollinson 1993, with data from this study)
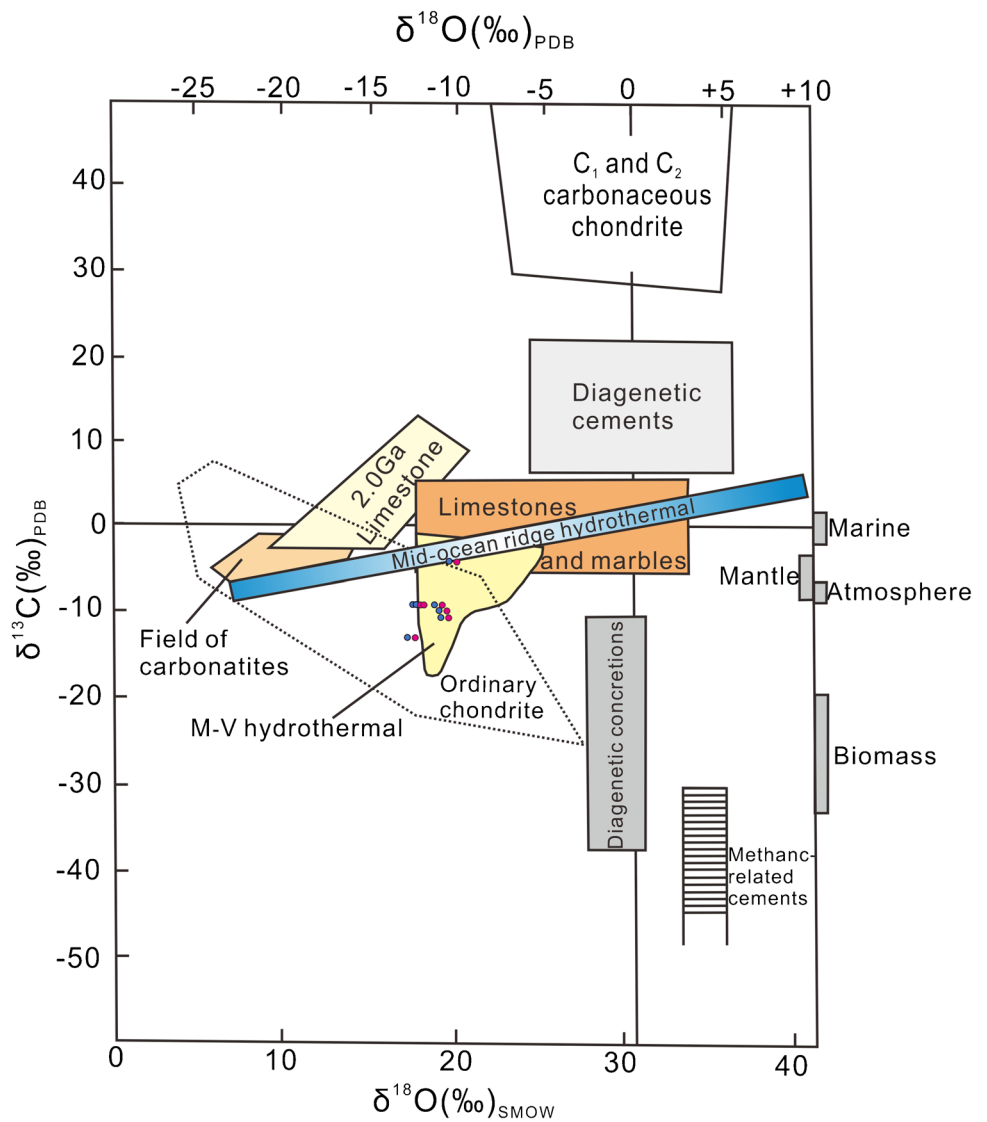
Formation, we suggest that the strong negative carbon isotope values of the carbonates from the Rongpo area were caused by the presence of (a series of) hotspots and the sea-level rise triggered by the "oceanic plateaus" (Larson 1991).

The Lhasa Block stabilized during the period from the Late Jurassic to the earliest Cretaceous, while the Indian Plate continued to move northwards, leading to elevated magmatic activity and the emplacement of volcanic rocks into the Sangxiu Formation (Zhu et al. 2005, 2007). Throughout the middle and later part of the Early Cretaceous, the regional oceanic crust underwent further rifting, leading to a maximum extension of the Neo-Tethys around 110 Ma, as demonstrated by palaeomagnetic data obtained from the northern Indian Plate and the Lhasa Plate (Liu and Einsele 1994). The U–Pb age dating of zircons from the Comai (Comei) igneous rocks in southeastern Tibet indicate that the mantle plume started in the Early Cretaceous (Zhu et al. 2009). At least two hotspots were found along the Cretaceous southern margin of the Indian Plate (Li and Jiang 2013). The occurrence of these hotspots likely coincided with the formation of the studied limestones, suggesting the possibility of an impact of hydrothermal fluid systems on the chemistry of the depositional environment and studied samples.

Correspondingly, the sea-level rise associated with the elevated production of the oceanic crust (Larson 1991) likely resulted in the rapid burial of organic carbon on enlarged continental margins, leading to a sharp relative decrease in ^{12}C and an increase in the ^{13}C in the seawater over a very short time. However, oceanic anoxic events may lead to a rapid positive shift in δ^{13}C, superimposed on these longer term trends, followed by a longer term trend toward a more negative δ^{13}C record which is less sensitive to short-term changes (Föllmi et al. 2006).

This oceanic spreading phase may explain the eustatic (relative) sea-level rise, during which more extended and deeper continental margins enabled the increased sequestration of organic carbon, locally resulting in the deposition of organic-rich black shales and mudstones.

This spreading phase may have allowed deep hydrothermal fluids to mix locally with the seawater, resulting in the strongly positive Eu anomalies and the abundant SiO_2 (average value 19.30%) observed in the limestone deposits.

Conclusions

Geochemical analyses were conducted on the Lower Cretaceous limestones of the Gyabula Formation from the Rongpo area in southern Tibet, including the study of the major and trace element concentrations, REE signatures, and the carbon and oxygen stable isotopic compositions of these rocks.

The m values calculated by major element, the Sr/Ba ratio, and the REE geochemistry (e.g. Ce/Ce*-La/Yb$_n$, Ce/Ce*-La/Ce$_n$, and Y/Ho) suggest that the studied limestones are deposited in a non-open marine environment. The observed Ce anomaly (Ce$_{anom}$ > − 0.1) and elevated V/(V + Ni) values suggest that these limestones were also deposited under anoxic depositional conditions.

Based on the presented REE data, we suggest that a passive tectonic setting during the Early Cretaceous marked the Neo-Tethys. However, large-scale plate movement of tectonic blocks of the Indian sub-continent resulted in an extensional phase of the Neo-Tethys Ocean and possibly in the short-term transgression recorded in the Rongpo area. This extensional tectonic phase may have been the ultimate cause of magmatic activity at that time, with the associated occurrence of hydrothermal fluids, as suggested by the sedimentary geochemical data presented in this study.

Declarations

Conflict of interest The authors declare no competing interests.

References

An W, Hu XM, Garzanti E (2017) Sandstone provenance and tectonic evolution of the Xiukang Mélange from Neotethyan subduction to India-Asia collision (Yarlung-Zangbo suture, south Tibet). Gondwana Res 41:222–234. https://doi.org/10.1016/j.gr.2015.08.010

Bau M, Dulski P (1996) Distributions of yttrium and rare-earth elements in the Penge and Kuruman iron-formation, Transvaal Supergroup, South Africa. Precambr Res 79:37–55. https://doi.org/10.1016/0301-9268(95)00087-9

Bau M, Dulski P (1999) Comparing yttrium and rare earths in hydrothermal fluids from the Mid-Atlantic Ridge: implications for Y and REE behaviour during near-vent mixing and for the Y/Ho ratio of Proterozoic seawater. Chem Geol 155:77–90. https://doi.org/10.1016/s0009-2541(98)00142-9

Bau M (1996) Controls on fractionation of isovalent trace elements in magmatic and aqueous systems: evidence from Y/Ho, Zr/Hf, and lanthanide tetrad effect. Contrib Mineral Petrol 123:323–333. https://doi.org/10.1007/s004100050159

Bertram CJ, Elderfield H (1993) The geochemical balance of the rare earth elements and neodymium isotopes in the oceans. Geochim Cosmochim Acta 57(9):1957–1986. https://doi.org/10.1016/0016-7037(93)90087-d

Boynton WV (1984) Cosmochemistry of the rare earth elements: Meteorolite studies. In: Henderson P (ed) Rare Earth Element Geochemistry. Elsevier Science Publishers, Armsterdam, 63–114

Brand U, Veizer J (1980) Chemical diagenesis of a multicomponent carbonate system–l: trace elements. J Sediment Petrol 50:1219–1236. https://doi.org/10.1306/212f7bb7-2b24-11d7-8648000102c1865d

Chen QQ, Lü ZX, Lun ZQ, Zhu YP (ed) (1993) Regional geology of Xizang Autonomous Region, Geological Report of Geology and Mineral Resources Ministry of the People's Republic of China (No. 31). Geological Publishing House, Beijing, 707pp. (in Chinese, with English contents)

Bolhar R, Van Kranendonk MJ (2007) A non-marine depositional setting for the northern Fortescue Group, Pilbara Craton, inferred from trace element geochemistry of stromatolitic carbonates. Precambr Res 155:229–250. https://doi.org/10.1016/j.precamres.2007.02.002

Bolhar R, Kamber BS, Moorbath S, Christopher MF, Whitehouse MJ (2004) Characterisation of early Archaean chemical sediments by trace element signatures. Earth Planet Sci Lett 222:43–60. https://doi.org/10.1016/j.epsl.2004.02.016

Bornemann A, Norris RD, Friedrich O, Beckmann B, Schouten S, Damsté JSS, Vogel J, Hofmann P, Wagner T (2008) Isotopic evidence for glaciation during the Cretaceous Supergreenhouse. Science 319:189–192. https://doi.org/10.1126/science.1148777

Chen L, Hu XM, Huang ZC (2007) Constrains from Early Cretaceous volcaniclastic sandstones in Southern Tibet on a volcanic event in the northern margin of the Indian continent. Acta Geologica Sinica 81(4): 501–510. (in Chinese) https://doi.org/10.3321/j.issn:0001-5717.2007.04.008

Chen X, Wang CS, Hu XM, Huang YJ (2008) The occurrence of iron in the Chuangde section of Gyangze, Southern Tibet: implications for the paleoceanography. Acta Geologica Sinica 82 (1): 77–84. (in Chinese) https://doi.org/10.3321/j.issn:0001-5717.2008.01.010

Coplen TB, Kendall C, Hopple J (1983) Comparison of stable isotope reference samples. Nature 302:236–238. https://doi.org/10.1038/302236a0

Cui Y, Gao LF, Leng CP, Jiang ZJ, Li K, Li ZF (2015) Analysis of Late Jurassic and Early Cretaceous sequence stratigraphy at Linxi section in Southern Tibet. Journal of Hebei United University (Natural Science Edition) 37(2): 89–93. (in Chinese) https://doi.org/10.3969/j.issn.2095-2716.2015.02.017

Danielson A, Möller P, Dulski P (1992) The europium anomalies in banded iron formations and the thermal history of the oceanic-crust. Chem Geol 97:89–100. https://doi.org/10.1016/0009-2541(92)90137-t

de Baar HJW (1983) The marine geochemistry of the rare-earth elements. Ph.D. Thesis, Massachusetts Institute of Technology and the Woods Hole Oceanographic Institution. Published thesis.

de Baar HJW (1991) On cerium anomalies in the Sargasso Sea. Geochim Cosmochim Acta 55(10):2981–2983. https://doi.org/10.1016/0016-7037(91)90463-F

Deng HW, Qian K (1993) Sedimentary geochemistry and environmental analysis. Gansu Science Technology Press, Lanzhou, 154 pp. (in Chinese)

Derry LA, Jacobsen SB (1990) The chemical evolution of Precambrian seawater: evidence from REEs in banded iron formations. Geochim Cosmochim Acta 54:2965–2977. https://doi.org/10.1016/0016-7037(90)90114-Z

Derry LA, Kaufman AJ, Jacobsen SB (1992) Sedimentary cycling and environmental change in the Late Proterozic: evidence from stable and radiogenic isotopes. Geochim Cosmochim Acta 56:1317–1329. https://doi.org/10.1016/0016-7037(92)90064-P

Derry LA, Brasier MD, Corfield RM, Rozanov AY, Zhuravlev AY (1994) Sr and C isotopes in Lower Cambrian carbonates from the Siberian craton: a paleoenvironmental record during the 'Cambrian explosion.' Earth Planet Sci Lett 128:671–681. https://doi.org/10.1016/0012-821X(94)90178-3

Derry LA (2010) A burial diagenesis origin for the Ediacaran Shuram-Wonoka carbon isotope anomaly. Earth Planet Sci Lett 294:152–162. https://doi.org/10.1016/j.epsl.2010.03.022

Douville E, Bienvenu P, Charlou JL, Donval JP, Fouquet Y, Appriou P, Gamo T (1999) Yttrium and rare earth elements in fluids from various deep-sea hydrothermal systems. Geochim Cosmochim Acta 63(5):627–643. https://doi.org/10.1016/S0016-7037(99)00024-1

Elderfield H (1988) The oceanic chemistry of the rare-earth elements. Philosophical Transactions of the Royal Society of London. Philosophical Transactions of the Royal Society of London. Series A, Mathematical and Physical Sciences 325(1583): 105–126. https://doi.org/10.1098/rsta.1988.0046

Föllmi KB, Godet A, Bodin S, Linder P (2006) Interactions between environmental change and shallow water carbonate buildup along the northern Tethyan margin and their impact on the Early Cretaceous carbon isotope record. Paleoceanography 21:1–16. https://doi.org/10.1029/2006PA001313

Frimmel HE (2009) Trace element distribution in Neoproterozoic carbonates as palaeoenvironmental indicator. Chem Geol 258:338–353. https://doi.org/10.1016/j.chemgeo.2008.10.033

Gansser A (1964) Geology of the Himalayas. Interscience Publication John Wiley and Sons Ltd., New York, p 289

Gao LF, Sun J, Wan XQ, Wang Y, Zuo WJ (2011) The discovery of calcareous nannofossils in Mesozoic marine strata at Gyangze, Southern Tibet and its significance. Marine Geology Frontiers 27(1): 33–37. (in Chinese) https://doi.org/10.16028/j.1009-2722.2011.01.006

Greaves MJ, Elderfield H, Sholkovitz ER (1999) Aeolian sources of rare earth elements to the Western Pacific Ocean. Mar Chem 68(1–2):31–38. https://doi.org/10.1016/S0304-4203(99)00063-8

Gromet LP, Dymek RF, Haskin LA, Korotev RL (1984) The 'North American Shale Composit': its compilation, major and trace element characteristics. Geochim Cosmochim Acta 48:2469–2482. https://doi.org/10.1016/0016-7037(84)90298-9

Guo LS, Liu YL, Liu SW, Cawood PA, Wang ZH, Liu HF (2013) Petrogenesis of Early to Middle Jurassic granitoid rocks from the Gangdese belt, Southern Tibet: Implications for early history of the Neo-Tethys. Lithos 179:320–333. https://doi.org/10.1016/j.lithos.2013.06.011

Haq BU (2014) Cretaceous eustasy revisited. Global Planet Change 113:44–58. https://doi.org/10.1016/j.gloplacha.2013.12.007

Haq BU, Hardenbol J, Vail PR (1987) Chronology of fluctuating sea level since Triassic. Science 235:1156–1167. https://doi.org/10.1126/science.235.4793.1156

Hatch JR, Leventhal JS (1992) Relationship between inferred redox potential of the depositional environment and geochemistry of the Upper Pennsylvanian (Missourian) stark shale member of the Dennis limestone, Wabaunsee County. Kansas USA Chemical Geology 99(1):65–82. https://doi.org/10.1016/0009-2541(92)90031-Y

Hu XM, Li J, An W, Wang JG (2017) The redefinition of Cretaceous-Paleogene lithostratigraphic units and tectonostratigraphic division in southern Tibet. Earth Science Frontiers 24(1): 174–194. (in Chinese) https://doi.org/10.13745/j.esf.2017.01.011

Hu XM, Wang CS, Li XH, Luba J (2006) Upper Cretaceous oceanic red beds in southern Tibet: lithofacies, environments and colour origin. Sci China, Ser D Earth Sci 49(8):785–795. https://doi.org/10.1007/s11430-006-0785-7

Hu XM, Jansa L, Wang CS (2008) Upper Jurassic-Lower Cretaceous stratigraphy in south-eastern Tibet: a comparison with the

western Himalayas. Cretac Res 29:301–315. https://doi.org/10.1016/j.cretres.2007.05.005

Huang Y, Cao HW, Li GM, Stefanie MB, Zhang Z, Dong L, Dai ZW, Lu L, Li YB (2018) Middle-Late Triassic bimodal intrusive rocks from the Tethyan Himalaya in South Tibet: geochronology, petrogenesis and tectonic implications. Lithos 318–319:78–90. https://doi.org/10.1016/j.lithos.2018.08.002

Huang Y, Zhang LK, Wei L, Li GM, Dong SL, Wu JY, Xia XB (2019) Petrogenesis of the Early Cretaceous Kada igneous rocks from Tethyan Himalaya: implications for initial break-up of eastern Gondwana. Geol J 54:1294–1316. https://doi.org/10.1002/gj.3227

Hudson JD (1977) Stable isotopes and limestone lithification. J Geol Soc 133(6):637–660. https://doi.org/10.1144/gsjgs.133.6.0637

Jenkyns HC (1980) Cretaceous anoxic events: from continents to oceans. J Geol Soc 137:171–188. https://doi.org/10.1144/gsjgs.137.2.0171

Jenkyns HC (2010) Geochemistry of oceanic anoxic events. Geochem Geophys Geosyst 11(3):1–30. https://doi.org/10.1029/2009GC002788

Jing YL, Zhang KX, Lin QX, Zhu YH, Wang ZP (2005) Sedimentary geochemistry characteristics and paleoenvironmental meaning of Helongshan Formation and Nanlinghu Formation in Meishan, Changxing County, Zhejiang Province. Geological Science and Technology Information 24(1): 35–40 (in Chinese) https://doi.org/10.3969/j.issn.1000-7849.2005.01.007

Jones B, Manning DAC (1994) Comparison of geochemical indices used for the interpretation of palaeoredox conditions in ancient mudstones. Chem Geol 111:111–129. https://doi.org/10.1016/0009-2541(94)90085-X

Klinkhammer G, German CR, Elderfield H, Greaves MJ, Mitra A (1994) Rare earth elements in hydrothermal fluids and plume particulates by inductively coupled plasma mass spectrometry. Mar Chem 45:179–186. https://doi.org/10.1016/0304-4203(94)90001-9

Kumar S, Bora S, Sharma UK, Yi K, Kim N (2017) Early Cretaceous subvolcanic calc-alkaline granitoid magmatism in the Nubra-Shyok valley of the Shyok Suture Zone, Ladakh Himalaya, India: evidence from geochemistry and U-Pb SHRIMP zircon geochronology. Lithos 277:33–50. https://doi.org/10.1016/j.lithos.2016.11.019

Lang XH, Liu D, Deng YL, Tang JX, Wang XH, Yang ZY, Cui ZW, Feng YX, Yin Q, Xie FW, Huang Y, Zhang JS (2018) Detrital zircon geochronology and geochemistry of Jurassic sandstones in the Xiongcun district, southern Lhasa subterrane, Tibet, China: implications for provenance and tectonic setting. Geological Magazine: 1–19 https://doi.org/10.1017/S0016756818000122

Larson RL (1991) Geological consequences of superplumes. Geology 19(10):963–966. https://doi.org/10.1130/0091-7613(1991)019%3c0963:GCOS%3e2.3.CO;2

Lawrence MG, Greig A, Collerson KD, Kamber BS (2006) Rare earth element and yttrium variability in South East Queensland waterways. Aquat Geochem 12:39–72. https://doi.org/10.1007/s10498-005-4471-8

Li D, Ling HF, Jiang SY, Pan JY, Chen YQ, Cai YF, Feng HZ (2009) New carbon isotope stratigraphy of the Ediacaran-Cambrian boundary interval from SW China: implications for global correlation. Geol Mag 146:465–484. https://doi.org/10.1017/s0016756809006268

Li D, Ling HF, Shields-Zhou GA, Chen X, Cremonese L, Och L, Thirlwall M, Manning CJ (2013) Carbon and strontium isotope evolution of seawater across the Ediacaran-Cambrian transition: evidence from the Xiaotan section, NE Yunnan, South China. Precambr Res 225:128–147. https://doi.org/10.1016/j.precamres.2012.01.002

Li GB, Luba J, Wan XQ, Pan M, Xiu D, Xie D (2011) Discovery of Radiolaria from Upper Cretaceous Oceanic Red Beds in Daba, Kangmar and its paleogeographic implication. Palaeogeogr Palaeoclimatol Palaeoecol 312:127–137. https://doi.org/10.1016/j.palaeo.2011.10.003

Li XH, Wei YS, Li YX, Zhang CK (2016) Carbon isotope records of the early Albian oceanic anoxic event (OAE) 1b from eastern Tethys (southern Tibet, China). Cretac Res 62:109–121. https://doi.org/10.1016/j.cretres.2015.08.015

Li JH, Jiang HF (2013) Global paleoplate reconstruction, petrographic paleogeography and paleoenvironment atlas. Geological Publishing House, Beijing, 127pp. (in Chinese)

Liu G, Einsele G (1994) Sedimentary history of the Tethyan basin in the Tibetan Himalayas. Geol Rundsch 83:32–61. https://doi.org/10.1007/BF00211893

Liu YL, Li GB (2012) Microfacies and sedimentary environments of Cretaceous fossil carbonate in Gamba, Southern Tibet. Geoscience 26(1): 22–35. (in Chinese) https://doi.org/10.3969/j.issn.1000-8527.2012.01.003

McLennan SM (1989) Rare earth elements in sedimentary rocks: influence of provenance and sedimentary processes. Geochemistry and Mineralogy of Rare Earth Elements, Reviews in Mineralogy 21:169–200. https://doi.org/10.1007/BF00209706

Michard A (1989) Rare earth element systematics in hydrothermal fluids. Geochim Cosmochim Acta 53:745–750. https://doi.org/10.1016/0016-7037(89)90017-3

Michard A, Albarède F, Michard G, Minster JF, Charlou JL (1983) Rare-earth elements and uranium in high-temperature solutions from East Pacific rise hydrothermal vent field (13°N). Nature 303:795–797. https://doi.org/10.1038/303795a0

Nan JY, Zhou DQ, Ye JL, Wang ZM (1998) Geochemistry of paleoclimate and paleo-ocean environment during Permian-Triassic in Guizhou Province. Acta Mineralogica Sinica 18(2): 239–249. (in Chinese) https://doi.org/10.1038/sj.cr.7290029

Neuhuber S, Wagreich M, Wendler I, Spötl C (2007) Turonian oceanic red beds in the Eastern Alps: concepts for palaeoceanographic changes in the Mediterranean Tethys. Palaeogeogr Palaeoclimatol Palaeoecol 251:222–238. https://doi.org/10.1016/j.palaeo.2007.03.049

Nothdurft LD, Webb GE, Kamber BS (2004) Rare earth element geochemistry of Late Devonian reefal carbonates, Canning Basin, Western Australia: confirmation of a seawater REE proxy in ancient limestones. Geochim Cosmochim Acta 68(2):263–283. https://doi.org/10.1016/S0016-7037(03)00422-8

Nozaki Y, Zhang J, Amakawa H (1997) The fractionation between Y and Ho in the marine environment. Earth Planet Sci Lett 148:329–340. https://doi.org/10.1016/S0012-821X(97)00034-4

Patzelt A, Li HM, Wang JD, Appel E (1996) Palaeomagnetism of Cretaceous to Tertiary sediments from southern Tibet: evidence for the extent of the northern margin of Indian prior to collision with Eurasia. Tectonophysics 259:259–284. https://doi.org/10.1016/0040-1951(95)00181-6

Piepgras DJ, Jacobsen SB (1992) The behavior of rare earth elements in seawater: precise determination of variations in the North Pacific water column. Geochim Cosmochim Acta 56(5):1851–1862. https://doi.org/10.1016/0016-7037(92)90315-A

Powell C McA, Roots SR, Veevers JJ (1988) Pre-breakup continental extension in East Gondwanaland and the early opening of the eastern Indian Ocean. Tectonophysics 155:261–283. https://doi.org/10.1016/0040-1951(88)90269-7

Rollinson HR (1993) Using geochemical data: evaluation, presentation, interpretation. Pearson Prentice Hall, England, 352pp.

Russell DA (1982) The mass extinctions of the Late Mesozoic. Sci Am 246(1):58–65. https://doi.org/10.1038/scientificamerican0182-58

Schlanger SO, Jenkyns HC (1976) Cretaceous oceanic anoxic events: causes and consequences. Geol Mijnbouw 55(3–4):179–184

Scholle PA, Arthur MA (1980) Carbon isotope fluctuations in Cretaceous pelagic limestones: potential stratigraphic and petroleum exploration tool. The American Association of Petroleum Geologists Bulletin 64(1):67–87. https://doi.org/10.1306/2F91892D-16CE-11D7-8645000102C1865D

Searle MP, Windley BF, Coward MP, Cooper DJW, Rex AJ, Rex D, Li TD, Xiao XC, Jan MQ, Thakur VC, Kumar S (1987) The closing of Tethys and the tectonics of the Himalaya. Geol Soc Am Bull 98:678–701. https://doi.org/10.1130/0016-7606(1987)98%3c678:TCOTAT%3e2.0.CO;2

Skelton PW, Spicer RA, Kelley SP, Gilmour I (2003) *The Cretaceous World*. Cambridge University Press, 360pp.

Tong HP, Chen DF (2012) First discovery and characterizations of late Cretaceous seep carbonates from Xigaze in Tibet. China Chinese Science Bulletin 33(57):4363–4372. https://doi.org/10.1007/s11434-012-5434-2

Veizer J, Ala D, Azmy K, Bruckschen P, Buhl D, Bruhn F, Carden GAF, Diener A, Ebneth S, Godderis Y, Jasper T, Korte C, Pawellek F, Podlaha OG, Strauss H (1999) $^{87}Sr/^{86}Sr$, $\delta^{13}C$ and $\delta^{18}O$ evolution of Phanerozoic seawater. Chem Geol 161:59–88. https://doi.org/10.1016/s0009-2541(99)00081-9

Van Kranendonk MJ, Webb GE, Kamber BS (2003) Geological and trace element evidence for a marine sedimentary environment of deposition and biogenicity of 3.45 Ga stromatolitic carbonates in the Pilbara Craton, and support for a reducing Archaean ocean. Geobiology 1:91–108. https://doi.org/10.1046/j.1472-4669.2003.00014.x

Wagreich M, Krenmayr HG (2005) Upper Cretaceous oceanic red beds (CORB) in the Northern Calcareous Alps (Nierental Formation, Austria): slope topography and clastic input as primary controlling factors. Cretac Res 26:57–64. https://doi.org/10.1016/j.cretres.2004.11.012

Wang CS, Xia DX, Zhou X, Chen JP, Lu Y, Wang GH, He ZW, Li XH, Wan XQ, Zeng QG, Ciren PB, Liu ZF (1996) Geology between the Indus-Yarlung Zangbo suture zone and the Himalaya Mountains, Xizang (Tibet), China. 30th International Geological Congress Field Trip Guide (T121/T387), Geological Publishing House, Beijing 5, 72 pp.

Wang CS, Li XH, Wan XQ, Tao R (2000) The Cretaceous in Gyangze, Southern Xizang (Tibet): redefined. Acta Geologica Sinica 74(02):97–107. (in Chinese)

Wang CX, Hu XM, Sarti M, Scott RW, Li XH (2005) Upper Cretaceous oceanic red beds in southern Tibet: a major change from anoxic to oxic, deep-sea environments. Cretaceous Res 26:21–32. https://doi.org/10.1016/j.cretres.2004.11.010

Wang C, Ding L, Liu ZC, Zhang LY, Yue YH (2017) Early Cretaceous bimodal volcanic rocks in the southern Lhasa terrane, south Tibet: age, petrogenesis and tectonic implications. Lithos 268–271:260–273. https://doi.org/10.1016/j.lithos.2016.11.016

Wang NW (1984) On the Palaeobiogeography and plate tectonics of Qinghai-Tibet Plateau. Journal of the Geology Institute of Chinese Academy of Geological Sciences 9:1–28 (in Chinese)

Wang YD, Huang CM, Sun BN, Quan C, Wu JY, Lin ZC (2014) Paleo-CO_2 variation trends and the Cretaceous greenhouse climate. Earth Sci Rev 129:136–147. https://doi.org/10.1016/j.earscirev.2013.11.001

Wang CS (2013) Environmental/ climate change in the Cretaceous greenhouse world: records from terrestrial scientific drilling of Songliao Basin and adjacent areas of China. Palaeogeogr Palaeoclimatol Palaeoecol 385:1–5. https://doi.org/10.1016/j.palaeo.2013.05.006

Wheat CG, Motti MJ, Rudnicki M (2002) Trace elements and REE composition of a low-temperature ridge-flank hydrothermal spring. Geochim Cosmochim Acta 66:3693–3705. https://doi.org/10.1016/S0016-7037(02)00894-3

Wright J, Schrader H, Holser WT (1987) Paleoredox variations in ancient oceans recorded by rare earth elements in fossil apatite. Geochim Cosmochim Acta 51:631–644. https://doi.org/10.1016/0016-7037(87)90075-5

Wynn TC, Read JF (2007) Carbon-oxygen isotope signal of Mississippian slope carbonates, Appalachians, USA: a complex response to climate-driven fourth-order glacio-eustasy. Palaeogeogr Palaeoclimatol Palaeoecol 256:254–272. https://doi.org/10.1016/j.palaeo.2007.02.033

Xia J, Wang LT, Zhong HM, Tong JS, Lu RK (2008) Mesozoic sedimentary environment and biological composition in Luozha, South Tibet. Geology of Anhui 18(4): 248–257, 263. (in Chinese) CNKI:SUN:AHDZ.0.2008–04–004

Xia J, Zhong HM, Tong JS, Lu RK (2005) Sedimentary facies and palaeogeography of the Lhozhag region in southern Xizang during the Jurassic and Cretaceous. Sedimentary Gelology and Tethyan Geology 25(3):8–17 (in Chinese)

Xia DX, Liu SK (1997) Stratigraphy (lithostratic) of Xizang Autonomous Region. Bureau of Geology and Mineral Resources of Xizang Autonomous Region, China University of Geosciences Press. 302 pp. (in Chinese)

Xiong GQ, Jiang XS, Cai XR, Wu H (2010) The characteristics of trace element and REE geochemistry of the Cretaceous mudrocks and shales from Southern Tibet and its analysis of redox condition. Advances in Earth Science 25(07): 730–745. (in Chinese) https://doi.org/10.11867/j.issn.1001-8166.2010.07.0730

Xu YL, Mao SZ (1992) Cretaceous-Early Tertiary calcareous nannofossils from Southern Xizang (Tibet) and their sedimentary environment. Acta Micropalaeontologica Sinica 9(4): 331–347. (in Chinese) https://doi.org/10.1007/BF02677081

Yang TS, Ma YM, Bian WW, Jin JJ, Zhang SH, Wu HC, Li HY, Yang ZY, Ding JK (2015) Paleomagnetic results from the Early Cretaceous Lakang Formation lavas: constraints on the paleolatitude of the Tethyan Himalaya and the India-Asia collision. Earth Planet Sci Lett 428:120–133. https://doi.org/10.1016/j.epsl.2015.07.040

Yang ZY, Shen WZ, Zheng LD (2009) Elements and isotopic geochemistry of Guadalupian-Lopingian boundary profile at the Penglaitan section of Laibin, Guangxi Province, and its geological implications. Acta Geologica Sinica 83(01): 1–15. (in Chinese) https://doi.org/10.3321/j.issn:0001-5717.2009.01.001

Yin G, Wang CS (1998) The composition of carbon and oxygen isotope and the discussion about the oceanic anoxic events in the Middle Cretaceous black shale, South Tibet. J Mineral Petrol 18(1): 95–101. (in Chinese) https://doi.org/10.1038/sj.cr.7290029

Yin A, Harrison TM (2000) Geologic evolution of the Himalayan-Tibetan orogen. Annu Rev Earth Planet Sci 28:211–280. https://doi.org/10.1146/annurev.earth.28.1.211

Yu GM, Lan BL, Wang CS (1983) A brief discussion on the Cretaceous deep-sea olistostrome and turbidite sedimentation in Gyangze, Xizang. Geology Paper Collections of Tibet Plateau 15:13–26 (in Chinese)

Yue LQ, Shi XY, Wang HZ (2003) Sedimentary environments of submarine fan of the Lower Cretaceous in Northern Himalayas. Journal of Palaeogeography 5(4): 391–403. (in Chinese) https://doi.org/10.3969/j.issn.1671-1505.2003.04.001

Yue LQ, Li YT, Shi XY (2006) Geologic characteristics and their hydrocarbon implication of black shales of the Lower Cretaceous in Kuco-Gamba Basin, Tibet. Journal of Palaeogeography 8(3): 307–316. (in Chinese) https://doi.org/10.7605/gdlxb.2006.03.002

Zhai DX, Zhang YS, Tian SG, Xing EY, Wu FM, Zhu CW, Jiang SY (2015) The Late Permian sedimentary environments of Linxi Formation in Xingmeng Area: constraints form carbon and oxygen isotopes and trace elements. Acta Geoscientica Sinica 36(3): 333–343. (in Chinese) https://doi.org/10.3975/cagsb.2015.03.08

Zhang J, Nozaki Y (1996) Rare earth elements and yttrium in seawater: ICP-MS determinations in the East Caroline, Coral Sea, and South Fiji basins of the western South Pacific Ocean. Geochim Cosmochim Acta 60(23):4631–4644. https://doi.org/10.1016/S0016-7037(96)00276-1

Zhang KJ, Li QH, Yan LL, Zeng L, Lu L, Zhang YX, Hui J, Jin X, Tang XC (2017) Geochemistry of limestones deposited in various plate tectonic settings. Earth Sci Rev 167:27–46. https://doi.org/10.1016/j.earscirev.2017.02.003

Zhang SS, Chen CH (1991) The study on Mg-Al ratio in sedimentary columnar samples from Central Pacific. Acta Oceanologica Sinica 13(1): 114–120. (in Chinese) https://doi.org/10.1007/BF03008874

Zhang SS (1988) Study on the Mg-Al content ratio in sedimentary rocks and its application. Bull Mineral Petrol Geochem 2:112–113. (in Chinese)

Zhao QY (1989) Marine geochemistry. Geological Publishing House, Beijing, 277 pp. (in Chinese)

Zhou ZC, Willems H, Xia J, Zhong HM, Tong JS (2004) Mesozoic trace fossils from Lhozhag area of Southern Tibet and their environmental significance. Acta Palaeontologica Sinica 43(2): 221–233. (in Chinese) https://doi.org/10.3969/j.issn.0001-6616.2004.02.006

Zhou ZC, Willems H, Zhang BG (1997) Marine Cretaceous-Paleogene biofacies and ichnofacies in southern Tibet, China, and their sedimentary significance. Mar Micropaleontol 32(1):3–29. https://doi.org/10.1016/S0377-8398(97)00011-X

Zhu DC, Chung SL, Mo XX, Zhao ZD, Niu YL, Song B, Yang YH (2009) The 132Ma Comei-Bunbury large igneous province: remnants identified in present-day southeastern Tibet and southwestern Australia. Geology 37(7):583–586. https://doi.org/10.1130/G30001A.1

Zhu DC, Pan GT, Mo XX, Liao ZL, Jiang XS, Wang LQ, Zhao ZD (2007) Petrogenesis of volcanic rocks in the Sangxiu Formation, central segment of Tethyan Himalayas: a probable example of plume-lithosphere interaction. J Asian Earth Sci 29:320–335. https://doi.org/10.1016/j.jseaes.2005.12.004

Zhu DC, Pan GT, Mo XX, Wang LQ, Liao ZL, Jiang XS, Geng QR (2005) SHRIMP U-Pb zircon dating for the dacite of the Sangxiu Formation in the central segment of Tethyan Himalaya and its implications. Chin Sci Bull 50:563–568. https://doi.org/10.1007/BF02897481